

---

# Chapter 15

# Sea Clutter

---

## Lewis B. Wetzel

Naval Research Laboratory (*retired*)

---

### 15.1 INTRODUCTION

---

For an operational radar, backscatter of the transmitted signal by elements of the sea surface often places severe limits on the detectability of returns from ships, aircraft, and missiles, navigation buoys, and other targets sharing the radar resolution cell with the sea surface. These interfering signals are commonly referred to as *sea clutter*, or *sea echo*. The search for a useful understanding of this important radar contaminant began with the collection and analysis of clutter data from operating radars, with the goal of establishing the relationship between clutter signals and the parameters of both the radar and the sea environment. Much of the earliest work took place during WWII and can be found in one of the comprehensive series of RADLAB volumes documenting the radar research that was done at that time.<sup>1</sup> But most of the clutter data from this period, and even into the 1960s, was collected in bits and pieces from isolated experiments, often with poor, incomplete, or misleading descriptions of the sea surface.

It would seem a simple matter to refine these results by using instrumentation radars operating over the wide variety of radar and environmental parameters encountered in practice. But while the parameters relating to the radar system and its configuration, such as frequency, cell size, polarization, grazing angle at the surface, etc., can be specified, selecting and quantifying the environmental parameters is quite another matter. First, it has not always been clear which environmental parameters are important. For example, wind speed certainly seems to affect clutter levels, but the correlation of clutter with, say, a ship's anemometer readings is often inconsistent. And although the state of agitation of the sea surface (*sea state*) appears to have a strong effect, it is a subjective measure and its relation to prevailing local winds is often uncertain. Moreover, it has been found that the temperatures of the air and the sea surface can affect the way in which measured wind speed is related to the generation of clutter-producing waves, yet the importance of these effects were unappreciated over most of the history of sea clutter measurements, so air and sea temperatures were seldom recorded. Finally, even if the importance of an environmental parameter has been recognized, it is often difficult (or too expensive) to measure it accurately in the field under real sea conditions.

While many aspects of sea clutter thus remained frustratingly ill-defined, the earlier work did disclose some general trends, such as the tendency of average clutter signal strengths at low to intermediate grazing angles to increase with the

grazing angle and the wind speed (or sea state), and generally to be greater for vertical polarization and in upwind/downwind directions. (For other reviews of sea clutter and its history, see Skolnik,<sup>2</sup> Nathanson,<sup>3</sup> and Long.<sup>4</sup>) Sea clutter is, however, a complex phenomenon, presenting various faces depending on the way the radar views the scene. For example, it is commonly noted that when viewed on an A scope (signal amplitude versus range), the appearance of sea clutter depends strongly on the size of the resolution cell, or *radar footprint*. For large cells, it appears *distributed* in range and may be characterized by a surface-averaged cross section with relatively modest fluctuations about a mean value. As the size of the resolution cell is reduced, clutter increasingly appears to contain sequences of isolated target-like, or *discrete*, returns that vary in time. At the higher resolutions, the discrete returns tend to stand well out of the background, occurring for both polarizations but most clearly evident with horizontal polarization at small grazing angles. These isolated returns are called *sea spikes* and are a common clutter component in this radar operating regime. Quite clearly, an understanding of sea clutter in all its aspects will be a considerable undertaking. Fortunately, a close relationship between radar and oceanography has grown up in the fields of remote sensing, leading to the accumulation of a large amount of information, both experimental and theoretical, about how scattering at radar frequencies relates to oceanographic variables. In many ways, this information serves as the basis of much of our current understanding of sea clutter.

In modeling sea clutter, there is a difference between a *theory*, which relates the physical scattering properties of the sea surface to the received signal, and a *characterization*, which provides a description of the sea clutter data in terms of a statistical model (e.g., Rayleigh, lognormal, Weibull, and K-distribution) that, although sometimes suggestive of physical processes in the underlying scattering, is of greater direct interest to the radar system designer in providing detection probabilities and false alarm rates.

Historically, attempts to provide a theoretical explanation of the observed behavior of clutter signals trace essentially from the work pursued during World War II and described in the well-known MIT Radiation Laboratory book mentioned above.<sup>1</sup> Unfortunately, the scattering models developed during this period, along with most of those published over the following decade, failed to account in any convincing way for the behavior of sea backscatter. In 1956, however, Crombie observed that at high-frequency (HF) wavelengths (tens of meters) scattering appeared to arise from a resonant interaction with sea waves of one-half of the incident wavelength, i.e., to be of the Bragg type.<sup>5</sup> Reinforced by the theoretical implications of various small waveheight approximations and wave-tank measurements under idealized conditions, the *Bragg model* was introduced into the microwave regime by many workers in the mid-1960s.<sup>6–8</sup> This produced a revolution in thinking about the origins of sea clutter because it involved the sea wave *spectrum*, thus forging a link between clutter physics and oceanography in what became the field of *radio oceanography*. However, fundamental conceptual problems in applying the Bragg hypothesis in microwave scattering, along with its inability to address significant aspects of measured sea clutter, have led through the years to continuing inquiry into the physical origins of sea scatter and how best to model it.<sup>9–14</sup> This being the case, speculation about physical models will be kept to a minimum in the sections on the empirical behavior of sea clutter. The problem of modeling sea scatter will be discussed separately in a later section.

## 15.2 THE SEA SURFACE

---

Close observation of the sea surface discloses a variety of features describable as wedges, cusps, waves, foam, turbulence, and spray, as well as breaking events of all sizes and masses of falling water. Any or all of these might contribute to the scattering of electromagnetic waves responsible for sea clutter. The basic oceanographic descriptor of the sea surface, however, is the *wave spectrum*, which says little about the details of these features, but contains a great deal of information about the sea surface in general and is central to the application of the Bragg scattering hypothesis. Accordingly, some tutorial material describing the spectral characterization of the sea surface is included in this section, along with a brief discussion of surface events such as wave breaking and other surface effects thought to contribute to the production of *sea spikes*.

There are basically two types of surface waves, *capillary* and *gravity*, depending on whether surface tension or gravity is the dominant restoring force. The transition between one and the other takes place at a wavelength of about 2 cm, so the smaller capillary waves supply the surface fine structure while gravity waves make up the larger and most visible surface structures. Sea waves have their origin primarily in the wind, but this does not mean that the “local” wind is a particularly good indicator of what the wave structure beneath it will be. In order to arouse the surface to its *fully developed* or *equilibrium* state, the wind must blow for a sufficient time (*duration*) over a sufficient distance (*fetch*). That part of the wave structure directly produced by these winds is called *sea*. But waves propagate, so even in the absence of local wind, there can be significant local wave motion due to waves arriving from far away, perhaps from a distant storm. Waves of this type are called *swell*, and since the surface over which the waves travel acts as a low-pass filter, *swell* components often take the form of long-crested low-frequency sinusoids.

**The Wave Spectrum.** The *ocean wave spectrum* describing the sea surface appears in several forms. If the time history of the surface elevation is monitored at a fixed point, the resulting time series may be processed to provide a *frequency spectrum*  $S(f)$  of the surface elevation, where  $S(f)df$  is a measure of the *energy* (i.e., square of the waveheight) of the waves in the frequency interval between  $f$  and  $f+df$ . Wave spectra have been measured in the open ocean primarily for gravity waves down to wavelengths of about 1 m. Open-ocean measurements of capillary wave spectra are especially difficult to perform.<sup>15,16</sup>

For a *gravity wave*, the frequency  $f$  and the wavenumber  $K$  are related by the dispersion relation

$$f = (1/2\pi)(gK)^{1/2} \quad (15.1)$$

where  $g$  is the acceleration of gravity and  $K = 2\pi/\Lambda$ , with  $\Lambda$  being the wavelength. Although each individual gravity wave obeys this relation, the waves at a point on the sea surface could come from any direction; so they are characterized by a two-dimensional propagation *vector* with orthogonal components  $K_x$  and  $K_y$ , where the  $K$  to be used in Eq. 15.1 is the magnitude  $K = (K_x^2 + K_y^2)^{1/2}$ . The wavenumber spectrum associated with  $S(f)$  is a function of the two components of  $K$  and is commonly written as  $W(K_x, K_y)$ . This is called the *directional wave spectrum* and expresses the asymmetries associated with winds, currents, refraction, isolated swell components, etc.

For a given source of asymmetry such as the wind, various parts of the spectrum will display different directional behaviors. For example, in a fully developed sea, the larger waves will tend to move in the direction of the wind while the smaller waves will be more isotropic. Directional spectra are more difficult to measure and are obtained by a variety of experimental methods, such as an array of wave staffs to measure surface heights over a matrix of points, a multiaxis accelerometer buoy, stereo photography, and even by processing radar backscatter signals. However, a frequency spectrum measured at a point can contain no knowledge of wave direction, so a wavenumber spectrum  $W(K)$  is often defined in terms of the frequency spectrum  $S(f)$  by the relation

$$W(K) = S(f(K))(df/dK) \quad (15.2)$$

with the relation between  $f$  and  $K$  given by Eq. 15.1. To account for the wind direction,  $W(K)$  is sometimes multiplied by an empirical function of  $K$  and direction  $\phi$  relative to the (up)wind direction.

Oceanographers have not always been in complete agreement about the form of the frequency spectrum. Nonequilibrium wave conditions, inadequate sampling times, poor ground truth, etc., can contaminate the data set from which empirical spectra are derived. However, by careful selection of data from many sources, ensuring that only equilibrium (fully developed) sea conditions were represented and the wind was always measured at the same reference height (usually taken as 10 meters), Pierson and Moskowitz<sup>17</sup> established a simple empirical spectrum that has proven popular and useful. It has the form

$$S(f) = Af^{-5} e^{-B(f_m/f)^4} \quad (15.3)$$

where  $g$  is the acceleration of gravity, and  $f_m = g/2\pi U$ , corresponding to the frequency of a wave moving with a velocity equal to the wind speed  $U$ ;  $A$  and  $B$  are empirical constants. This spectrum is illustrated in Figure 15.1 for several wind speeds. The effect of increasing wind speed is simply to move the low-frequency cutoff to lower frequencies along the high-frequency  $f^{-5}$  asymptote. (It should be noted that most of the oceanographers' spectra are based on measurements at relatively low frequencies and so cannot be taken seriously at frequencies above about 2 Hz. Nevertheless, these spectral forms are often used up to 20 Hz or greater in predicting radar clutter under the Bragg hypothesis.)

Converting this frequency spectrum into an isotropic wavenumber spectrum through Eq. 15.2 results in a spectrum of similar form, only with a  $K^{-4}$  asymptote. Phillips<sup>17</sup> derived this asymptotic behavior on dimensional grounds, and a widely used simplification, obtained by replacing the smooth peak in Figure 15.1 by a sharp cutoff, is generally referred to as the *Phillips Spectrum*:

$$\begin{aligned} W(K) &= 0.005K^{-4} & K > g/U^2 \\ &= 0 & K < g/U^2 \end{aligned} \quad (15.4)$$

where the cutoff wavenumber corresponds to the frequency  $f_m$  of the peak in Eq. 15.3. Opposed to this highly simplified form are increasingly complex spectra based on more careful empirical studies<sup>18</sup> as well as more sophisticated theoretical considerations.<sup>19</sup>

In discussing the characterization of the sea surface by its spectrum, it must be kept in mind that the spectrum is a highly averaged description of how the *energy* of the surface is distributed among the wavenumbers, or frequencies, of the waves present on it.

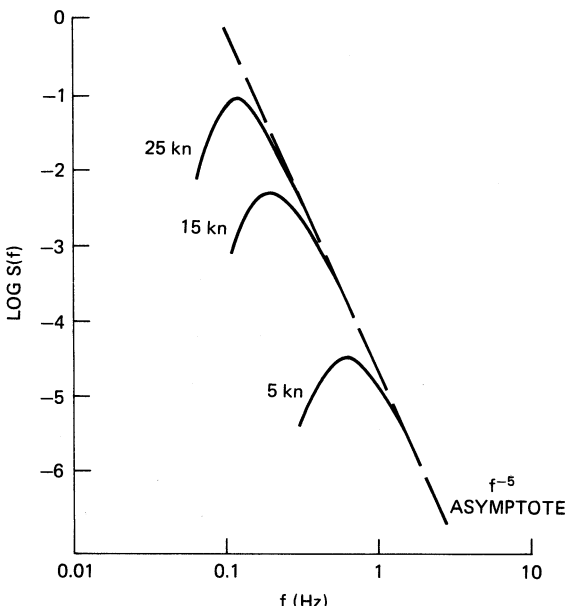


**FIGURE 15.1** Sea wave frequency spectra of the Pierson-Moskowitz type, representing fully developed seas (after W. J. Pierson and L. Moskowitz<sup>16</sup> © American Geophysical Union 1968)

Since the phases of these waves are lost, the spectrum gives no information about the detailed morphology of the surface itself, i.e., about the complex surface features that are responsible for the scattered field. This point will be raised again as we go along.

**General Sea Descriptors.** The shape of the curves in Figure 15.1 indicates that the sea wave system is sharply peaked, so it should be possible to get a rough idea of the behavior of the major waves on the surface by taking the values of *period* ( $1/f$ ) and *wavelength* ( $2\pi/K$ ) defined at the spectral peak. These values are assigned to a wave satisfying the dispersion relation Eq. 15.1 and having a phase velocity  $C = 2\pi f/K$  equal to the wind speed  $U$ . By using Eq. 15.1, the period  $T'$  and wavelength  $\Lambda'$  thereby defined take the form

$$T' = 0.64U \quad \Lambda' = 0.64U^2 \quad (15.5)$$

where  $U$  is in meters per second. For example, the largest waves in a fully developed sea for a 15 kt (8 m/s) wind will have a wavelength of about 135 ft (41 m) with a period of 5 s.

The statistical distribution of waveheights on the ocean surface is quite close to gaussian, with a mean square height that can be obtained by integrating the waveheight spectrum over all frequencies (or wavenumbers). For spectra resembling those in Figure 15.1, the rms waveheight is given approximately by

$$h_{\text{rms}} = 0.005U^2 \text{ m} \quad (15.6)$$

The rms waveheight contains contributions from all the waves on the surface, but very often it is the peak-to-trough height for the higher waves that is of major interest. This is certainly the case for a ship in a seaway or in the shadowing of the surface at low radar grazing angles. The *significant height*, or peak-to-trough height of the one-third highest waves, provides such a measure. It is denoted by  $H_{1/3}$  and is taken to be about six times the spectral rms amplitude (see, e.g., Kinsman,<sup>20</sup> Fig. 8.4-2). For a 15-kt wind, this is only about 2 ft, but for gale-force winds of 40 kt, it rises to almost 15 ft, which is a rather formidable sea.

Looking at the sea, an observer might describe what is seen in terms of a subjective *state of the sea*, e.g., “smooth,” “rough,” or “terrifying!” If these descriptions are listed in order of severity and assigned numbers, these numbers define a *sea state*. A similar numerical scale exists for wind speeds, the *Beaufort wind scale*, with numbers about an integer higher than the corresponding sea state. But it is seldom used in reference to sea clutter.

There are, then, two numbers commonly used to indicate the activity of the sea surface: a subjective sea state and a measured wind speed. Only when the wind has sufficient *fetch* and *duration* to excite a *fully developed* sea, can a waveheight be unambiguously associated with it. The surface descriptors generally used in connection with sea clutter—sea state, wind speed, and its associated equilibrium waveheight—are given in Table 15.1, with the wind speed in knots, the significant waveheight in feet, and the duration/fetch required for a fully developed sea in hours/nautical mile. It is of interest to note that the median wind speed over the world’s oceans is about 15 kt, corresponding to sea state 3.

**Breaking Waves and Other Surface Disturbances.** The observable features of the sea surface that best suggest an origin for the sharp localized radar returns called *sea spikes* are surface events that are themselves sharply localized, events including breaking waves of all sizes, induced either by the wind or by nonlinear interactions among wave systems. Large-scale breaking waves display two characteristic behaviors—*spilling*, in which an unstable wave peak unravels, and *plunging*, where the peak curls over on itself and crashes onto the front face as a cascade of water masses, ending in a chaotic jumble.<sup>20</sup> Another different event is the *microbreaker*, a small, transient shock front induced by a puff of wind or another wave. As noted earlier, highly averaged wave spectra cannot disclose the morphology of such surface features, and, unfortunately, physical oceanography is still unable to provide a generally satisfactory description or characterization of wave breaking.<sup>21</sup> Nevertheless, there are two useful heuristic parameters relating elements of a breaking wave scene to wind speed. Whitecap density is a visible tracer of breaking wave activity and has a power-law dependence on wind speed

TABLE 15.1 Sea-Surface Descriptors

Sea State	Wind Speed, kt	Waveheight $H_{1/3}$ , ft	Duration/fetch, h/nmi
1 (smooth)	< 7	1	1/20
2 (slight)	7–12	1–3	5/50
3 (moderate)	12–16	3–5	15/100
4 (rough)	16–19	5–8	23/150
5 (very rough)	19–23	8–12	25/200
6 (high)	23–30	12–20	27/300
7 (very high)	30–45	20–40	30/500

given by  $\rho_{wb} \sim U^{3.5}$ .<sup>22</sup> The average length of a breaking wavefront moving at speed  $c$  also depends on wind speed and is given by a parameter  $\Lambda(c)$ .<sup>23</sup> These parameters will appear again later when we discuss some of the more recent models for sea clutter. An additional feature of small-scale breaking, or other strongly nonlinear events, is the appearance of “parasitic” or “bound” capillaries attached to the event and moving with it.<sup>20,24</sup> They tend to be small-amplitude features, localized and narrow-band.

### 15.3 EMPIRICAL BEHAVIOR OF SEA CLUTTER

---

Sea clutter is a function of many parameters, some of them showing a complicated interdependence, so we emphasize again that it is not an easy task to establish its detailed behavior with a great deal of confidence or precision. For example, in a proper sea clutter measurement, the polarization, radar frequency, grazing angle, and resolution cell size will have been specified. Then the wind speed and direction must be measured at a reference altitude, and if the results are to be compared with those of other experimenters, the proper *duration* and *fetch* should be available to ensure standardization to equilibrium sea conditions. Since these measured winds are related to the wind structure at the surface through the atmospheric boundary layer, the shape of this layer must be determined by measuring the air and sea temperatures. To complicate the picture still further, it has been found that sea clutter can be dependent on the direction of the long waves, which includes *swell* in the measurement area, so ideally the *directional wave spectrum* should be measured as well. Obviously, it is unlikely that all of these environmental parameters will be recorded with precision in every (or even *any*) sea clutter measurement; so considerable variability in the basic conditions under which sea clutter data are collected by different experimenters can be expected. It is of interest to note that in many of the reported measurements of sea clutter, particularly in the older literature, wide inconsistencies between wind speed and waveheight may be found. For example, a wind speed of 5 kt might be reported with waveheights of 6 ft, or 20-kt winds with 2-ft waves. These pairings are not consistent with the values for an equilibrium sea described in Table 15.1 and indicate the unnoticed or unrecorded presence of heavy swell or highly nonequilibrium wind conditions or both. Even with all the variables properly specified, recorded clutter data can be spread over a wide dynamic range, especially at low grazing angles.

Since sea clutter is generally viewed as a surface-distributed process, the basic clutter parameter is taken to be the normalized radar cross section (NRCS),  $\sigma^0$ , of the surface, commonly referred to as *sigma zero* and expressed in decibels relative to  $1 \text{ m}^2/\text{m}^2$ . It is obtained experimentally by dividing the measured radar cross section of an illuminated patch of the surface by a normalizing area, so differences in the definition of this area can lead to inconsistencies among various reports of NRCS measurements. Scattering from any distributed target involves the product of the transmitting and receiving system footprints integrated over the target. These footprints cover exactly the same area for a monostatic radar and will depend on the pulse- and beamwidths, the range, and the grazing angle. If the footprints are assumed to be of the *cookie-cutter* type (constant amplitude falling sharply to zero at the half-power points), then the relation between the actual radar clutter cross section  $\sigma_c$ , as inferred from the received power via the *radar equation*, and the NRCS  $\sigma^0$  is given by

$$\sigma^0 = \sigma_c / A_f \quad (15.7)$$

where for a radar with an antenna beamwidth  $B$  and rectangular pulse of length  $\tau$ , viewing the surface at range  $R$  and grazing angle  $\psi$ , the area  $A_f$  is either

$$A_f = \pi(BR)^2/4 \sin \psi \quad (15.8)$$

for beam-limited conditions (e.g., continuous-wave (CW) or long-pulse radar at high grazing angles) or

$$A_f = (c\tau/2)BR/\cos \psi \quad (15.9)$$

for pulse-width-limited conditions (e.g., short-pulse radar at low grazing angles).

Real radars do not produce cookie-cutter footprints, however, since the antenna beam will have a complex profile and the pulse might be shaped. For this reason, an effective  $A$  must be obtained from a surface integration of the actual amplitude profile of the footprint, which will tend to result in a smaller value of  $A$  than that defined by Eq. 15.8 or Eq. 15.9. This will produce larger values of  $\sigma^0$  as derived from measured values of  $\sigma_c$  by Eq. 15.7. Most experimenters use the half-power beamwidth in Eq. 15.8 or Eq. 15.9, with an error that is usually only 1 or 2 dB.

**Clutter Statistics.** Summaries of clutter measurements made before about 1970 may be found in several of the standard reference books on radar<sup>2,3</sup> and radar clutter.<sup>4</sup> Among the programs of this period, the most ambitious was that pursued in the late 1960s at the Naval Research Laboratory (NRL),<sup>25</sup> in which an airborne four-frequency radar (4FR), operating with both horizontal and vertical polarizations at UHF (428 MHz), L band (1228 MHz), C band (4455 MHz), and X band (8910 MHz), made clutter measurements upwind, downwind, and crosswind in winds from 5 to 50 kt for grazing angles between 5° and 90°. The system was calibrated against standard metal spheres dropped from aircraft, and wind speeds and waveheights were recorded in the measurement areas from ship instruments.

Typically, samples of  $\sigma^0$  for a given set of radar and environmental parameters are scattered over a wide range of values and in the NRL measurements were organized into probability distributions of the type shown in Figure 15.2. The data, represented by the solid line, are plotted on normal probability paper with Rayleigh and log-normal distributions shown for comparison (dashed lines). The ordinate is the *percent of time for which the abscissa is exceeded*, and the abscissa is the value of  $\sigma^0$  as defined by Eq. 15.7, with  $A$  taken from Eq. 15.8 or Eq. 15.9 as appropriate. This particular distribution is representative of clutter from a relatively large radar footprint (pulse length about 0.5  $\mu$ sec or 75 meters) measured at intermediate grazing angles (20° to 70°) for moderate wind speeds (about 15 kt). It is Rayleigh-like but shows a tendency toward log-normal behavior for the larger cross sections. From a detailed statistical analysis of the NRL 4FR data, Valenzuela and Laing<sup>26</sup> concluded that, for this data at least, the distributions of sea clutter cross sections were intermediate between the Rayleigh and log-normal distributions.

Organizing the data samples into probability distributions makes the *median* (50%) value a convenient statistical measure of the clutter cross section. But many investigators process their data to provide the *mean* value, and because the conversion of a *median* to a *mean* requires knowledge of the probability distribution function, care must be taken to avoid ambiguity in comparing the measurements of different experimenters. The original analysis of the NRL 4FR data was based on *median* cross sections and the assumptions of the cookie-cutter antenna beam embodied in Eqs. 15.8 and 15.9.<sup>25-27</sup> In later presentations of this data,<sup>28</sup> the *median* values of  $\sigma^0$

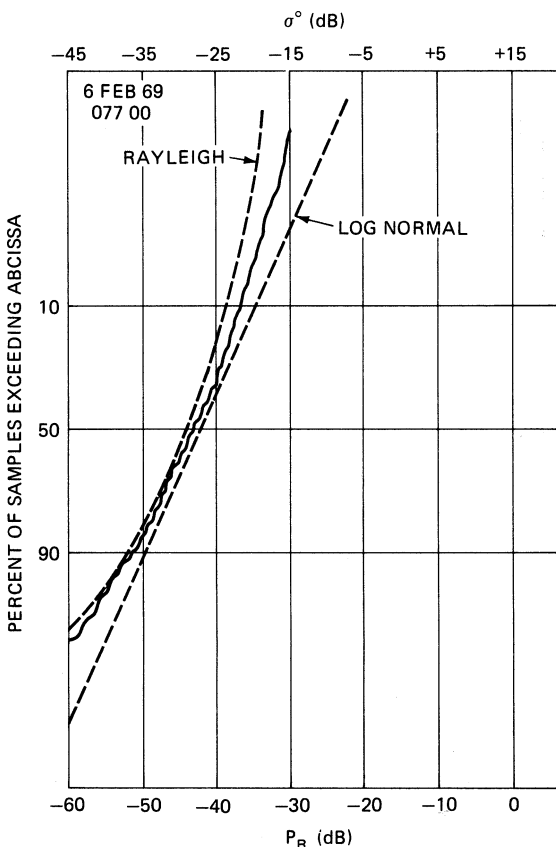


**FIGURE 15.2** An example of the probability distribution of sea clutter data (from J. C. Daley et al.<sup>25</sup>)

were replaced by *means*, raising them by about 1.6 dB, and the area *A* in Eq. 15.7 was redefined in terms of a more realistic tapered footprint, adding another 1 to 2 dB. This means that there can be a difference of 3 to 4 dB between the earlier and later presentations of the same data, and since these results have been widely used and quoted, it is important to ensure that the proper definition of  $\sigma^0$  is being used when comparing them with clutter data that has been taken by other experimenters or in using these results in clutter predictions.

Figure 15.2 shows that even for intermediate grazing angles in the range 20°–70° the sea clutter distribution departs from strictly Rayleigh. At lower grazing angles, and particularly for narrow pulse widths, the presence of *sea spikes* or other non-gaussian behavior may be accommodated by one of the multiparameter or compound distributions that express an excess of higher returns, such as the Weibull and K-distributions. The latter was introduced to characterize the particular behavior of low-grazing-angle clutter seen in a marine environment.<sup>29</sup> Its success is very likely due to its relation to the Rice distribution, which describes the statistics of steady signals in noise, thus reflecting the statistics of “target-like” sea spike returns in a Rayleigh background.<sup>30</sup>

**General Trends.** Being the first really comprehensive collection of clutter data over a wide range of radar frequencies, the 4FR program produced many plots showing the dependence of sea clutter on grazing angle, frequency, polarization, wind direction, and wind speed. However, comparison of these plots with others made both earlier and later shows the extent of the variations to be found in sea clutter measurements reported by different investigators for exactly the same set of parameters. This is seen clearly in Figure 15.3a and b, which compares the grazing-angle dependence of X-band clutter data for wind speeds in the neighborhood of 15 kt obtained from four sources: NRL 4FR<sup>28</sup> (these are *mean* results for upwind directions and include the antenna corrections mentioned above), aircraft measurements by Masuko et al.<sup>31</sup> (also in the upwind direction), and summaries of data taken from books on radar systems by Skolnik<sup>2</sup> and Nathanson.<sup>3</sup> The discrepancies between the different data sets can be accounted for, at least in part, as follows. The older data summaries were based on published measurements from various sources in which there is no specification of wind direction. It may, therefore, be assumed that these data represent some kind of average of upwind, downwind, and crosswind directions. As will be seen, this average is about 2 to 3 dB smaller than the upwind returns. Moreover, the *early* NRL 4FR data was used liberally in the older data summaries, and it was noted above that there is a difference of 3 to 4 dB between the early and later presentations of the same NRL 4FR data, the *latter* being used in Figure 15.3a and b. With these corrections, the curves might show closer agreement. Nevertheless, it is clear that uncritical use of published clutter data could lead radar systems designers to choose sea clutter estimates many dB apart for the same conditions.

The NRL 4FR data set is unique in that no other program has reported measurements made over so wide a range of frequencies, grazing angles, and wind speeds at the same time. Figure 15.4 shows the *trends* for both vertically and horizontally polarized

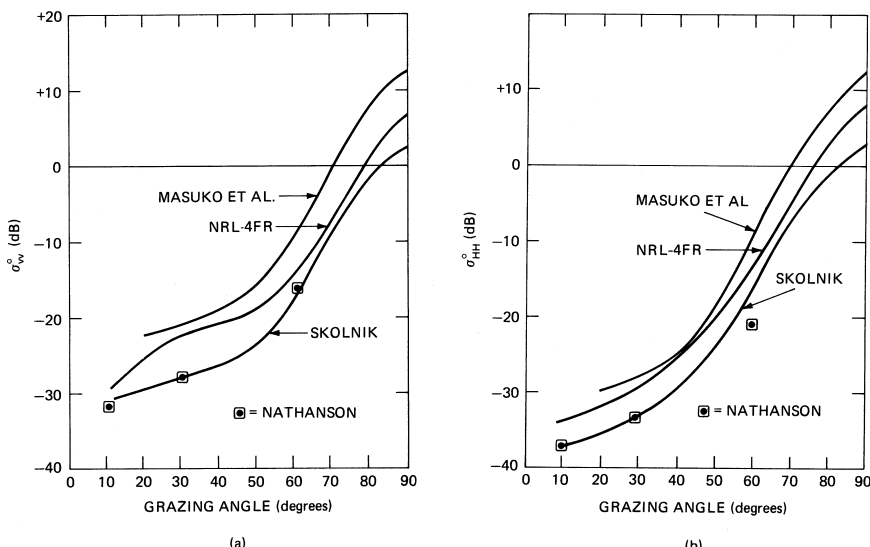


**FIGURE 15.3** Comparison of X-band clutter data from different sources for a nominal wind speed of 15 kn: (a) vertical polarization and (b) horizontal polarization (based on data from H. Masuko et al.,<sup>31</sup> NRL 4FR,<sup>25</sup> M. I. Skolnik,<sup>2</sup> and F. E. Nathanson<sup>3</sup>)

sea clutter over a range of grazing angles down to  $5^\circ$ . The curves represent the *centers* of  $\pm 5$  dB bands that contain the major returns for the three higher frequencies (L, C, and X bands—the UHF returns were a few decibels lower) and wind speeds above about 12 kt. The major differences in sea clutter for the two polarizations are seen to lie in the range of grazing angles between about  $5^\circ$  and  $60^\circ$ , where the horizontally polarized returns are smaller. This difference is found to be emphasized at both lower wind speeds and lower frequencies. The cross sections approach each other at high angles ( $>50^\circ$ ) and, for the higher microwave frequencies, at low angles ( $<5^\circ$ ) as well. In fact, for grazing angles less than a few degrees and moderate to strong wind speeds, observers have reported that at X band and at the higher sea states the horizontally polarized returns can exceed the vertically polarized returns.<sup>1,32,33</sup>

The NRL 4FR system permitted transmission and reception on orthogonal polarizations so that data could be collected for cross-polarized sea clutter. These returns tended to have a weak dependence on grazing angle and were always smaller than either of the like-polarized returns, lying in the cross-hatched region shown on Figure 15.4.

It is informative to compare measurements at different frequencies by different investigators in different parts of the world under similar wind conditions. Figure 15.5 displays measurements of vertically polarized sea clutter down to a grazing angle of  $20^\circ$  for wind speeds of about 15 kt from three independent experiments using airborne radars at C-, X-, and K-band frequencies.<sup>31,34,35</sup> Although there is no assurance that

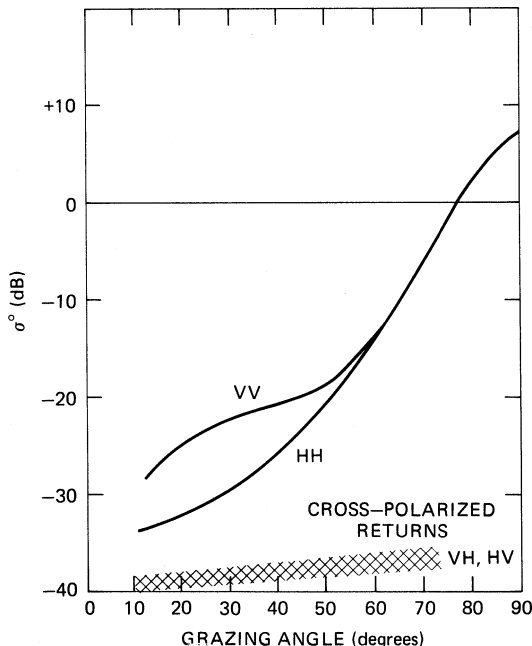


**FIGURE 15.4** General trends in clutter behavior for average wind speeds (about 15 kt) based on NRL 4FR data. Plots represent L-, C-, and X-band data within  $\pm 5$  dB.

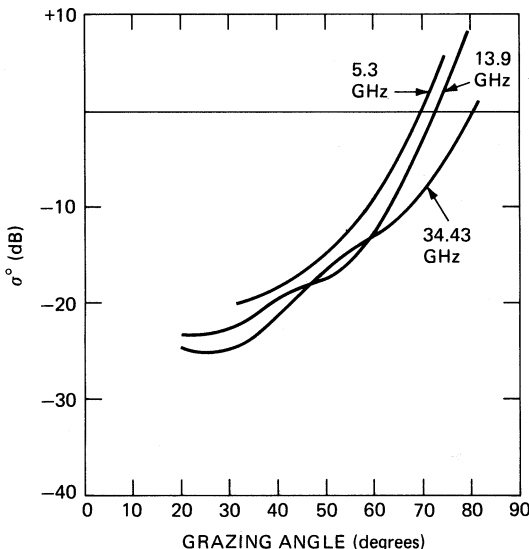


**FIGURE 15.5** Frequency dependence of sea clutter for wind speeds of about 15 kt: 5.3 GHz, Feindt;<sup>34</sup> 13.9 GHz, Schroeder;<sup>35</sup> and 34.4 GHz, Masuko<sup>31</sup>

all these measurements were made over fully developed seas, it is clear that there is a rather strong consistency among them, which reinforces the observation made in reference to Figure 15.4 that the frequency dependence of sea clutter at intermediate grazing angles is weak at microwave frequencies from L to K band.

**Dependence on Wind Speed and Direction.** Experimentally, the relation between sea clutter and wind speed is complex and uncertain, it having been found to depend on almost all of the parameters that characterize sea clutter: frequency, grazing angle, polarization, the state of the sea surface, the direction and speed of the wind itself, and even on whether the measurements are made from an aircraft or a tower platform.<sup>36</sup>

A common way to organize clutter data is to seek the best straight-line fit (linear regression) between clutter cross sections in decibels and the log of the wind speed (or some other parameter). This, of course, *imposes* a power-law relation between the variables:  $\sigma^0 \sim U^n$ , where  $n$  is determined by the slope of the line. An example is shown in Figure 15.6.<sup>37</sup> On the other hand, while the totality of the NRL 4FR results appeared to show saturation for wind speeds above about 20 kt, the high and low-to-moderate wind-speed data were collected at different times in different places under different conditions of sea-surface development, and discrepancies between the two data sets for common wind speeds have weakened the evidence for saturation.<sup>38</sup> Other investigators deny that it is even possible to express wind dependence in the form of a power law, proposing the existence of a kind of threshold wind speed, below which clutter virtually vanishes and above which the clutter level rises rapidly toward a saturation value.<sup>18</sup> This is indicated by the curves in Figure 15.7, where the straight lines correspond to various power laws and the curved lines derive from

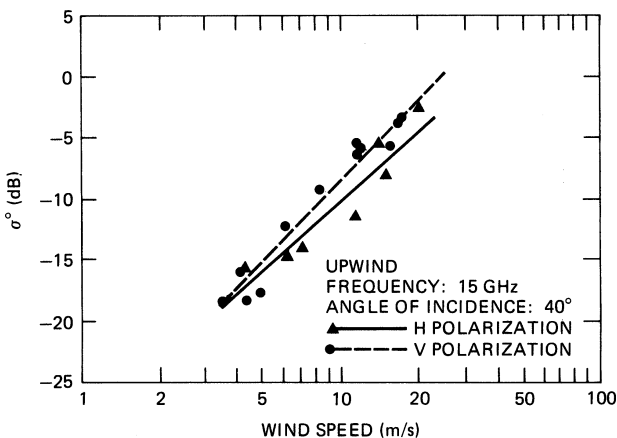


**FIGURE 15.6** Sea clutter from a tower platform with power-law wind-speed dependence defined by linear regression (angle of incidence = 90° grazing angle) (after A. H. Chaudhry and R. K. Moore,<sup>37</sup> © IEEE 1984)

wave spectrum considerations.<sup>18</sup> It is possible to find examples of data that appear to follow such behavior while at the same time being expressed as a power law by brute linear regression, as illustrated in the tower data shown in Figure 15.8.<sup>37</sup> This behavior is not uncommon.

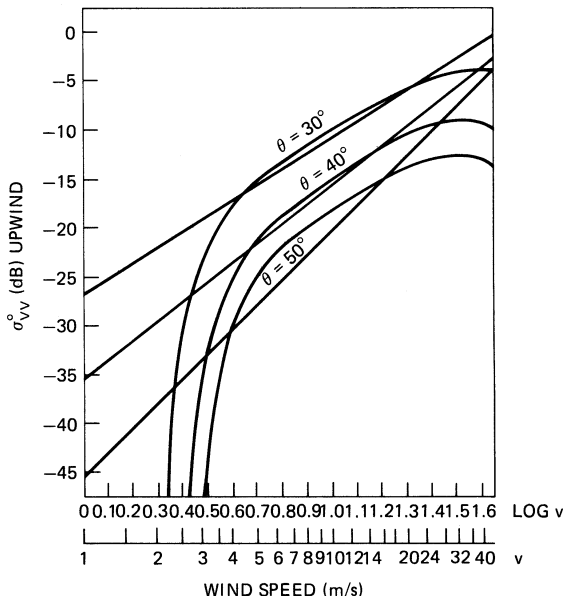


**FIGURE 15.7** A hypothetical wind-speed dependence of sea clutter (curved traces) compared with various power laws (straight lines) (derived from W. J. Pierson and M. A. Donelan<sup>18</sup> © American Geophysical Union 1987)

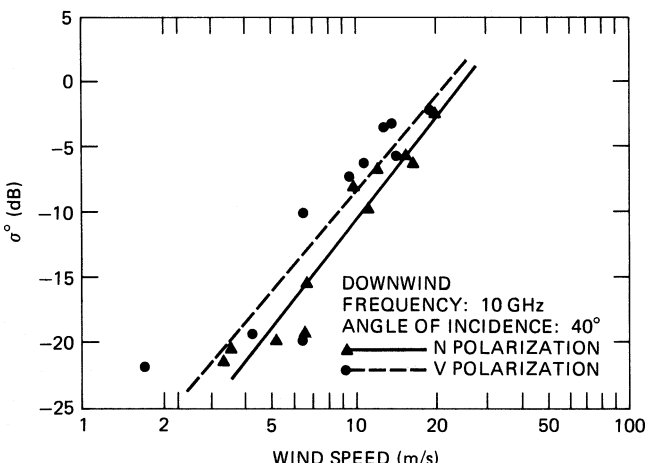
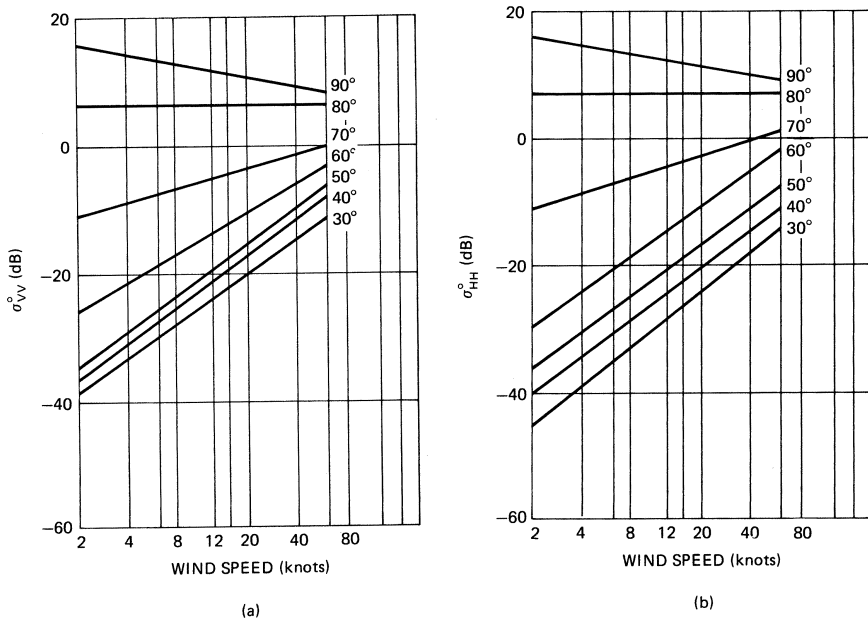


FIGURE 15.8 Example of forcing a power-law fit (compare data points with those in Figure 15.6) (after A. H. Chaudhry and R. K. Moore<sup>37</sup> © IEEE 1984)

Nevertheless, the imposition of a power-law relation provides a convenient way to visualize trends in the behavior of sea clutter with wind speed. The various aircraft measurements referred to above,<sup>31,34,35</sup> augmented by data from a tower in the North Sea,<sup>36,37</sup> were used as the basis of the power-law plots of  $\sigma^0$  as functions of wind speed and grazing angle shown in Figure 15.9a,b. These plots suggest how sea clutter for a given frequency (X band), wind direction (upwind), and polarization behaves with wind speed and grazing angle. However, examination of the actual data points underlying these linear regressions show point scatter that sometimes resembles Figure 15.6, sometimes Figure 15.8, and sometimes neither, so these straight lines cover up considerable uncertainty. In fact, it appears that there is no simple functional dependence of sea clutter on wind speed that can be established with any confidence from existing data, although most investigators would probably agree that the behavior of microwave sea clutter with wind speed at intermediate grazing angles can be roughly described as follows: for light winds (less than 6 to 8 kt) sea clutter is weak, variable, and ill defined; for intermediate winds (about 12 to 25 kt), it can be described roughly by a power law of the type found in Figure 15.6; and for strong winds (above about 30 kt), there is a tendency for it to level off. In fact, the convergence of the lines in Figure 15.9a,b with increasing wind speed suggests that the reflectivity of the sea surface is tending toward Lambert's law, for which there is no dependence on grazing angle, frequency, or polarization but only on surface albedo, or average reflectivity.

In several of the experiments referenced above, the dependence of sea backscatter on angle relative to the wind direction was found by recording the radar return from a spot on the surface while flying around it in a circle. Figure 15.10a,b gives an example of this behavior for grazing angles of about 45° and wind speeds close to 15 kt.<sup>31</sup> The figures contain results obtained independently by three different groups. The behavior shown here is representative of that found generally: sea clutter is strongest viewed upwind, weakest viewed crosswind, and of intermediate strength viewed downwind, the total variation being about 5 dB. Other studies corroborate this behavior.<sup>39</sup>



**FIGURE 15.9** A representation of X band, upwind clutter behavior with wind speed and grazing angle:  
(a) vertical polarization and (b) horizontal polarization

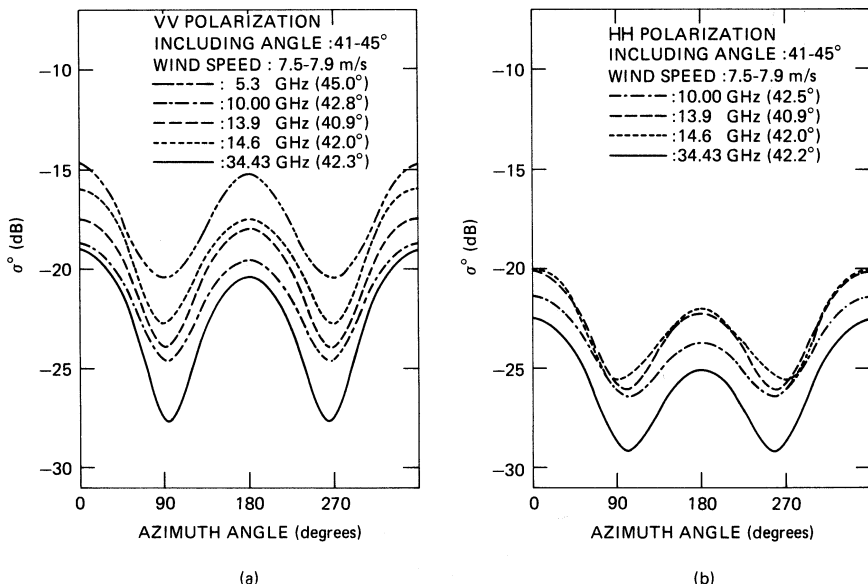


**FIGURE 15.10** Dependence of clutter on wind direction: nominal wind speed, 15 kt; grazing angle about 45°; upwind, 0°, 360°; and downwind, 180° (after H. Masuko et al.,<sup>37</sup> © American Geophysical Union 1986)

**Sea Clutter at High Grazing Angles.** The top lines in Figure 15.9a,b correspond to clutter at a grazing angle of  $90^\circ$ , that is, for a radar looking straight down. On a strictly empirical basis, the clutter cross section at this angle is only weakly dependent on frequency, has a maximum of about 15 dB at zero wind speed (at least for the antenna beamwidths and experimental configurations reported), and falls off gradually as the wind picks up. Scattering at high grazing angles is commonly regarded as a form of specular scattering from tilted facets of the surface, so it is of interest to note that there appears to be a small range of angles in the neighborhood of  $80^\circ$  for which the cross section is almost completely independent of wind speed. Since these angles correspond to complements of the common rms sea slope angles of about  $10^\circ$ , it might be argued that as the wind increases, the clutter *decrease* due to increasing surface roughness is balanced by a clutter *increase* due to an increasing population of scattering facets. This line could, therefore, be regarded as the boundary separating the *specular* regime, where the cross section is decreased by surface roughness, from the *rough-surface* regime, where the cross section increases with surface roughness. It should further be noted that clutter measurements at these high grazing angles will be relatively sensitive to the averaging effects of wide antenna beamwidths, which could become a source of ambiguity in aircraft measurements at the lower radar frequencies.

**At Low Grazing Angles.** At low grazing angles, below mean sea slope angles of about  $10^\circ$ , sea clutter takes on a different character. The sharp target-like clutter peaks known as *sea spikes* begin to appear on A-scope presentations,<sup>1,32,40,41</sup> and the probability distributions assume a different form.<sup>30,42</sup> Figure 15.11a and b show the presence of sea spikes in 125-second time histories of returns from a fixed spot, measured off the coast of Florida with a variable-resolution X-band radar looking into moderate (a) and calm (b) seas at a  $1.5^\circ$  grazing angle.<sup>24</sup> Notice that the *appearance* of the sea spikes is very similar for both moderate and weak wind conditions, although the *amplitudes* differ by almost 40 dB, and the vertically polarized returns appear to be somewhat broader, while the horizontally polarized returns are more spiky, particularly for short pulses in calm seas. These are all characteristics of sea clutter at low grazing angles.

The probability distributions of low grazing angle sea clutter change with wind speed. Examples may be found in the measurements by Trizna of low-angle sea clutter using high-resolution (40-ns) shipboard radar in both the Atlantic and the Pacific oceans.<sup>42</sup> The probability distributions of the clutter cross sections were plotted in the manner shown in Figure 15.12, which shows the distributions of horizontally polarized X-band data at a  $3^\circ$  grazing angle for low, medium, and high wind speeds (in order from left to right). The low-wind trace corresponds to a Rayleigh distribution; the other segmented traces are two-parameter Weibull distributions defined by different parameter pairs. It is clear that the behavior is different and considerably more complex than that shown in Figure 15.2 for higher grazing angles and wider pulses. From the character of the data, Trizna interprets these three-segment traces as showing primarily receiver noise in the lowest branch, distributed (spatially homogeneous) clutter in the middle branch, and genuine sea spikes in the branch containing the highest cross sections, some of which exceed  $1000 \text{ m}^2$ . For the higher wind speeds and fully developed seas encountered in the North Atlantic, the percentage of sea spikes in this population was found to grow as the 3.5th power of the wind speed, which, interestingly, is the same wind-speed dependence shown by the percentage of whitecaps seen on the surface,<sup>22</sup> which, as noted in Section 15.2, are tracers for breaking waves.

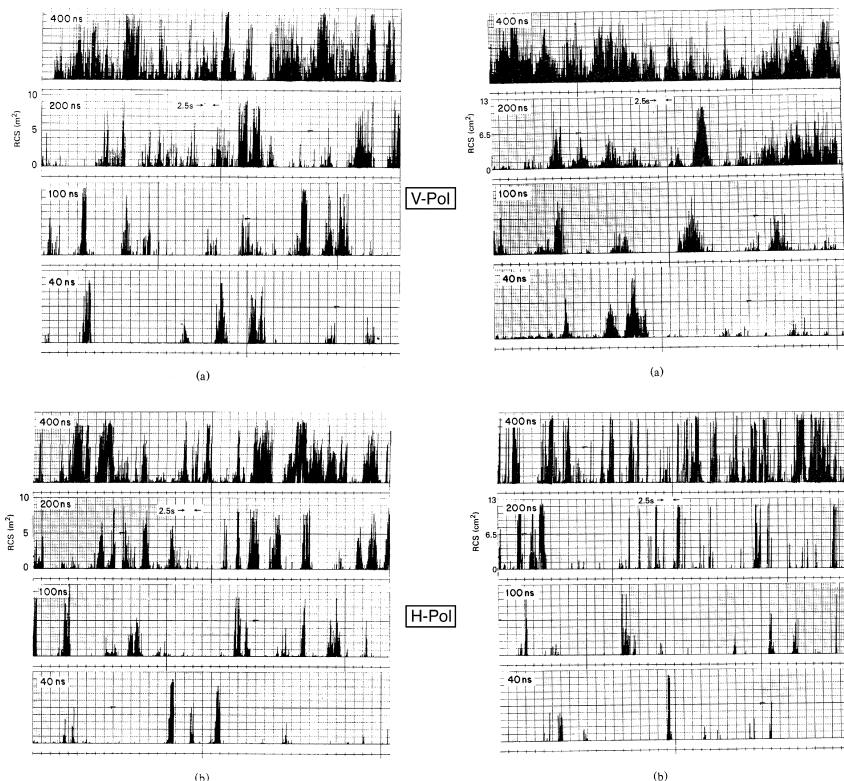


**FIGURE 15.11** Sea spikes at X band,  $1.5^\circ$  grazing angle, and various pulse widths: (a) sea state 3 and (b) sea state 1. Note equal amplitudes at the two polarizations and a 40 dB difference in clutter strength between moderate and weak winds. (from J.P. Hansen and V. F. Cavaleri<sup>41</sup>)

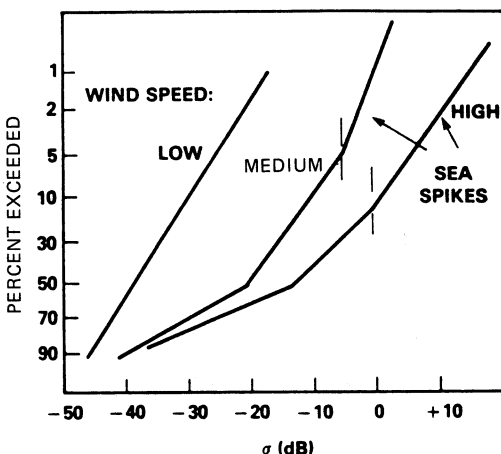


**FIGURE 15.12** Examples of clutter probability distributions at low grazing angles (after D. Trizna<sup>42</sup>)

In comparing statistical results, it should be kept in mind that to the extent that the sea surface may be viewed as a stationary homogeneous process, as it generally is over the duration and spatial extent of any particular experimental event, the scattering cross section may be said to be *ergodic*, which means that the statistical results obtained by time averaging from a small cell are equivalent to an ensemble average from a larger cell, provided that the number of “samples” is the same in the two cases.<sup>43</sup> For this reason, the statistical implications of experimental data can be properly compared only if the details of the sampling procedure are specified. However, the number of samples in most of the experimental results shown thus far have been sufficiently large that the differences between, for example, Figures 15.2 and 15.12, may be considered real and related to differences in grazing angle rather than in resolution cell size. In fact, distributions closely resembling those in Figure 15.12 were obtained much earlier from similar measurements with considerably broader pulse widths.<sup>44</sup> Other measurements have continued to confirm the differences that emerge in A-scope appearance and statistical description of the clutter in this regime of low grazing angles.<sup>45</sup> Some attempts to describe the physical origin of these phenomena will be discussed in Section 15.4 below.

**At Very Low Grazing Angles.** There is some evidence that sea clutter might drop off more sharply below a *critical angle* in the neighborhood of a degree or so.<sup>4</sup> This critical angle, or *critical range* for a radar at a fixed height, has been observed from time to time since first noted in early observations of sea clutter.<sup>1</sup> The critical angle has been ascribed to interference between direct and (perfectly) reflected rays at the scattering *targets* responsible for the clutter signal, although these targets remain unspecified.<sup>46</sup> Although this simple picture could produce the  $R^{-7}$  decay that is sometimes observed, a critical angle often fails to materialize, and when it does, it need not show an  $R^{-7}$  decrease with range (equivalent to a fourth-power dependence on grazing angle).<sup>1</sup> An alternative explanation for this behavior, applicable at the higher microwave frequencies, has been suggested based on a *threshold-shadowing* model for upwind and downwind directions.<sup>12,47</sup> This model implies a sharp decrease in the average cross section for grazing angles below a few degrees. In crosswind directions with the radar looking along the troughs of the major waves, a much milder shadowing function will apply, so there should be a clear distinction between the upwind-downwind and crosswind behavior of sea clutter at very low grazing angles.

Examples of clutter behavior at these very low angles may be found in independent measurements at relatively high wind speeds by Hunter and Senior off the south coast of England<sup>48</sup> and by Sittrop off the west coast of Norway.<sup>49</sup> Their results for orthogonal directions relative to the wind are shown in Figure 15.13, along with the predictions of a conventional shadowing function<sup>50</sup> and the threshold-shadowing function.<sup>47</sup> It would appear that a combination of conventional shadowing (which goes as the first power of the grazing angle) across the wind, and threshold shadowing in upwind and downwind directions, can account for the observed behavior of this very low-angle clutter quite well. The decay law for very low-angle clutter should, therefore, depend on the viewing angle relative to the wind direction, so it might occur with powers between the first and the fourth. This is just what has been observed.<sup>51</sup> It should be remarked, however, that *shadowing* at low grazing angles is a complex phenomenon (see below), and the physical origin or even the existence of a critical angle is still open to question. Moreover, there is relatively little good data on very low-angle clutter for other than X-band frequencies, so the general behavior of sea clutter in this angular regime remains uncertain.

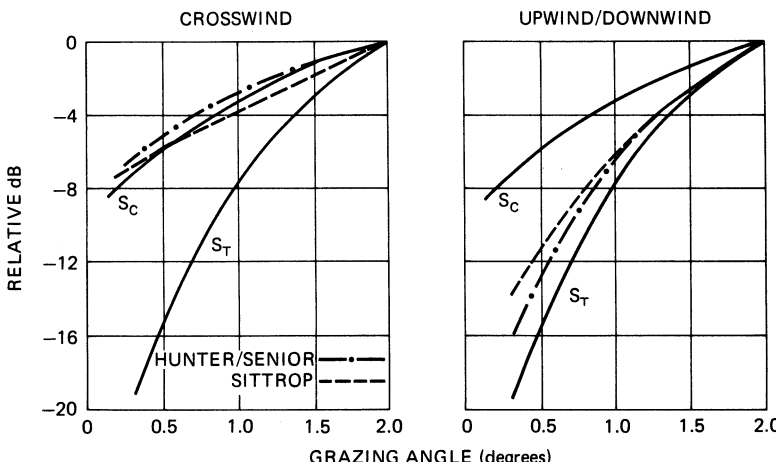


**FIGURE 15.13** Differential behavior of very low-angle clutter for orthogonal wind directions:  $S_c$  is a conventional shadowing function;<sup>50</sup>  $S_T$  is a threshold-shadowing function.<sup>47</sup> (after data from I. M. Hunter and Senior<sup>48</sup> © IEEE 1966 and H. Sittrop<sup>49</sup>)

**At HF and Millimeter-Wave Frequencies.** All the measurements described above were made at microwave frequencies between UHF (428 MHz) and K<sub>a</sub> band (35 GHz). High-frequency (HF) radars usually operate in the frequency range between about 5 and 30 MHz, corresponding to wavelengths between 60 and 10 m, respectively. Since the operation of such radars takes place either by the ground wave or over ionospheric (*sky-wave*) paths spanning great ranges, the grazing angles tend to be small (between 0° and 20°). For these wavelengths and grazing angles, measurements by Crombie indicate that the scattering from the sea surface was the result of scattering from sea waves of one-half the radar wavelength,<sup>5</sup> i.e., “Bragg” scatter. In the years since these early measurements, there has been considerable activity in the field of HF radar and HF clutter,<sup>52,53</sup> and the results can be summarized as follows: For vertical polarization, the major energy of the HF clutter signal appears in spectral lines displaced to either side of the carrier frequency by the frequency of sea waves having a wavelength equal to half the HF wavelength  $\lambda$  (in meters). The relative strengths of the plus and minus lines are determined by the proportion of advancing and receding Bragg-resonant wave components in the clutter cell. Provided the wind speed is greater than about  $\sqrt{3}\lambda kt$  (with  $\lambda$  in meters) and the sea is fully developed, the clutter cross section  $\sigma^0$  is about -29 dB and is relatively independent of wind speed and frequency. (The definition of  $\sigma^0$  in HF radar is complicated by problems in properly defining antenna gains for ground-wave and sky-wave paths and by propagation effects due to the ionosphere.) The clutter spectrum tends to fill in around and between the lines as the wind picks up. For horizontal polarization (which is possible only for sky-wave paths over which the plane of polarization can be rotated by the Earth’s magnetic field), the cross section is much smaller and shows the characteristic fourth-power decay with a decreasing grazing angle. For these HF wavelengths of tens of meters, the sea is relatively flat, and the scattering laws are simple. A detailed discussion of HF radar may be found in Chapter 20.

At the other end of the potentially useful radar spectrum, in the millimeter-wave band, the few published measurements of radar clutter lead to the conclusion that millimeter-wave backscatter behaves in much the same manner as backscatter at the lower microwave frequencies. This was suggested by the K-band curves shown in Figure 15.5 for moderate wind speeds and further supported by some older shipboard data at frequencies between 9 and 49 GHz.<sup>54</sup> It should be noted that for maritime radars clutter signal paths lie close to the sea surface, where the atmospheric and water-vapor densities are highest. This means that at these higher frequencies the clutter signal will be strongly affected by atmospheric absorption effects, and consequently the surface-related cross section inferred from the received signal strength in any given measurement will depend upon the path length. Moreover, the role of sea spray in both scattering and absorption will certainly be more important than at the lower microwave frequencies.

It is difficult to find clutter data at frequencies above K<sub>a</sub> band, although H- and V-polarized returns at 95 GHz at a grazing angle of 1° were reported, both with values close to -40 dB.<sup>55,56</sup>

**The Spectrum of Sea Clutter.** The scattering features producing sea clutter are associated with a surface subject to several types of motion. The features themselves may be moving with small group or phase velocities over this surface while the surface itself is moved, in turn, by the orbital velocities of the larger waves passing across it, or the feature may be advected at the velocity of the wave system supporting it. The scatterers might even be detached from the underlying surface, as in the plumes emitted at the crests of breaking waves, and move at speeds greater than the wave system itself.<sup>57</sup> At higher radar frequencies and in strong winds, the possibility of scattering from spray carried by the wind field above the surface must be considered. All of this complex motion shows up in a doppler shift imparted to the scattered electromagnetic wave. Unfortunately, there is as yet little detailed physical understanding of the complicated phenomenology of sea clutter spectra.

Measurements of microwave clutter spectra for real seas have been reported in the literature for aircraft measurements of the spectral shape alone,<sup>58,59</sup> fixed-site shore measurements showing a shift in the spectral peak,<sup>60,61</sup> and measurements from ships at intermediate grazing angles.<sup>45</sup> Other measurements of sea clutter spectra include those made at much lower frequencies in the HF band, as described in the last section; those made under artificial conditions in wave tanks,<sup>62</sup> whose application to real-sea conditions is uncertain; and those from other fixed-sites at high resolution and short averaging times, to be discussed later.

As it turns out, microwave sea clutter spectra have a rather simple form at the lower grazing angles. Figure 15.14 illustrates typical spectral behavior at the two polarizations, based on data collected by Pidgeon for C-band clutter looking upwind at a few degrees grazing.<sup>60</sup>

The peak frequency of the upwind spectrum appears to be determined by the peak orbital velocity of the largest sea waves, plus a wind-dependent velocity increment containing, but not entirely explained by, wind-induced surface currents. This *peak orbital velocity* is taken to be that of the major waves and may be obtained in terms of the significant height  $H_{1/3}$  and peak period  $T'$  (Section 15.2) from the expression

$$V_{\text{orb}} = \pi H_{1/3} / T' = 0.15 U \text{ (m/s)} \quad (15.10)$$

The approximate dependence on wind speed  $U$  was found by substituting  $H_{1/3} = 6 h_{\text{rms}}$  from Eq. 15.6, assuming a *fully developed sea*, and  $T'$  from Eq. 15.5. To this, there must

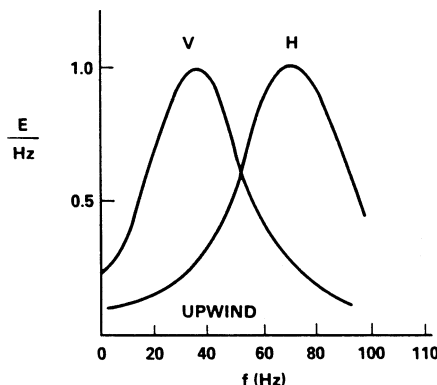


**FIGURE 15.14** Qualitative behavior of doppler spectra of sea clutter looking upwind at low grazing angles (after C-band measurements by V. W. Pidgeon<sup>60</sup> © American Geophysical Union 1968)

be added a wind-drift velocity of about 3% of  $U$  and a fixed *scatterer* velocity (which appears to be about 0.25 m/s in the X- and C-band measurements<sup>60,61,63</sup>). Summing these components yields the virtual doppler velocity at the peak of the clutter spectrum for the particular case of a *vertically polarized X- or C-band* radar looking upwind at low grazing angles:

$$V_{\text{vir}} = 0.25 + 0.18 U \text{ (m/s)} \quad (15.11)$$

(As noted earlier, care must be taken whenever wind speed is used to parameterize a process that depends on waveheight. There is an unambiguous relation only for a fully developed sea in the absence of swell.) The remaining properties of the clutter spectrum can now be discussed in terms of  $V_{\text{orb}}$  and  $V_{\text{vir}}$ . For example, the spectral peak for *horizontal* polarization follows a similar linear dependence on  $U$ , only with a coefficient lying somewhere between 0.20 and 0.30, as may be noted in the sketch shown in Figure 15.14. The reasons for the differences between the spectra for the two polarizations are not as yet clear, although the tendency of the H-polarization spectra to lie at a higher frequency is likely due to the preferential source of H-polarization returns in faster-moving wave structures.<sup>45,64</sup>

The (half-power) *width*  $\Delta$  of the clutter *velocity* spectrum is quite variable, depending on such things as radar polarization and sea conditions. It seems most closely related to the peak orbital velocity given by Eq. 15.10. Nathanson shows a plot containing spectral widths at both polarizations from several investigators over a wide assortment of unspecified sea conditions.<sup>65</sup> The points are widely scattered, but the dependence on wind speed is given roughly, with a rather large variance, by the expression  $\Delta \sim 0.24 U$  (m/s), which is just the orbital velocity in Eq. 15.10 with a coefficient about halfway between the values for vertical ( $\sim 0.15$ ) and horizontal ( $\sim 0.30$ ) polarization. For look directions away from upwind, the peak doppler follows a cosine dependence quite closely, going to zero at crosswind aspects and turning negative downwind.<sup>29</sup> The *width* of the spectrum appears to remain relatively constant.

The details of the clutter spectrum show little dependence on either the radar frequency or the grazing angle, at least for angles less than about  $10^\circ$ . In reviewing the results of measurements at four frequencies—UHF, L, C, and X bands—Valenzuela and Laing<sup>59</sup> noted a relatively weak tendency of clutter bandwidth to decrease with increases in frequency between the UHF and X bands and grazing angles between  $5^\circ$  and  $30^\circ$ . Since both of these variations can likely be accompanied by a change in the size of the radar footprint on the surface, they might be due to a dependence on resolution cell dimensions, although the other workers found that the pulse length had little effect on clutter bandwidth for values between about 0.25 and 10  $\mu$ sec.

Spectra obtained with *short* averaging times disclose something of the origins of the clutter spectrum. Figure 15.15 is a sequence of 0.2 second spectra obtained by Keller et al.<sup>66</sup> with a coherent vertically polarized X-band radar operating at a grazing angle of  $35^\circ$  and a resolution cell size of about  $10 \text{ m}^2$ . The zero-doppler reference in this figure was located arbitrarily at  $-116 \text{ Hz}$ . The spread along each line

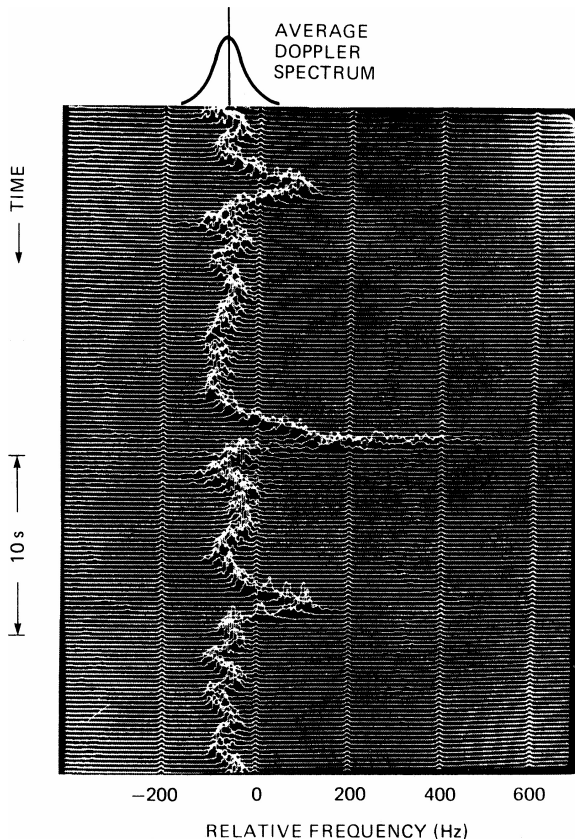


**FIGURE 15.15** Short-time averaged doppler spectra at X band for an intermediate grazing angle of  $35^\circ$ ; spectra computed at 0.2 sec intervals (shallow-water data is from a fixed site on a pier.) (from W. C. Keller et al.<sup>66</sup>)

is due to the small-scale wave motions on the surface, while the larger meanders are induced by the velocities of large waves moving through the measurement cell. The wind speed was about 8 m/s, and a doppler shift of 100 Hz corresponds to a radial velocity of 1.6 m/s. The average clutter spectrum expected for this wind speed and grazing angle, with bandwidth estimated from Eq. 15.10, is included in the sketch shown in Figure 15.15. The large spectral spike appearing in the center of the display is no doubt due to a wave breaking in or close to the measurement cell. The doppler velocity for this spike suggests a peak scatterer velocity about equal to the wind speed, which would correspond to the velocity of the longest waves on the surface. Although such events are relatively rare in a fixed area of  $10 \text{ m}^2$ , they should occur quite frequently within a large surveillance cell and might often have large scattering cross sections associated with them. Similar records may be found in reference Ward et al.<sup>29</sup>

### Other Environmental Effects.

**Rain.** Early evidence of the effect of rain on sea clutter was mainly anecdotal; for example, radar operators would report that sea clutter tends to decrease when it starts to rain. However, there has been little in the way of reliable, quantitative experimental information about the interaction between rain and wind-driven sea clutter in the open ocean. Laboratory measurements by Moore et al.<sup>67</sup> with artificial "rain" suggested that for light winds the backscatter level increased with the rain rate, while for heavy winds rain made little difference. Extensive measurements at  $K_u$  band in the open ocean tended to confirm this behavior.<sup>68</sup>

In measurements in natural rain over Chesapeake Bay, Hansen<sup>69</sup> found that even a light rain (2 mm/h) changes the spectral character of sea clutter at moderate wind speeds (6 m/s) by introducing a significant high-frequency component. He also found some evidence in support of the radar operators, at least for the low grazing angles and horizontal polarizations with which most shipboard radars operate. Figure 15.16 compares the correlation function of sea clutter (X band, low grazing angle, H polarization) with and without rain for a 15-kt wind speed and a rain rate of 4 mm/h. The sharp decrease in correlation time in the presence of rain reflects the broadening of the clutter spectrum, although generally there appears to be little quantitative information about the effect of rain on the spectrum of sea clutter.

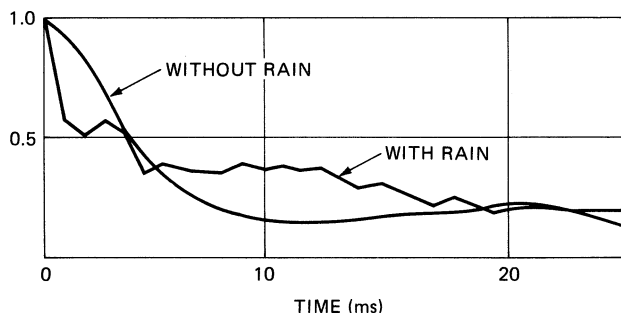


**FIGURE 15.16** Effect of rain on the correlation function of wind-driven sea clutter: X band, horizontal polarization, wind speed 15 kt, rain rate 4 mm/h (from J. P. Hansen<sup>69</sup>)

The production of sea clutter by rain falling on a “calm” surface in the absence of wind was also investigated by Hansen, with the results shown in Figure 15.17.<sup>69</sup> A high-resolution X-band radar (40-ns pulse, 1° beamwidth), operating at a grazing angle of about 3°, viewed the backscatter from a fixed spot on the windless surface of Chesapeake Bay as the rain steadily increased from 0 to 6 mm/h. The cross sections for vertical and horizontal polarizations were quite different for low rain rates but tended to merge at a rain rate of about 6 mm/h. The magnitude of this *splash* cross section rose to a  $\sigma^0$  of about -40 dB, corresponding to highly averaged wind-induced cross sections at this grazing angle for winds of about 10 kt. Further laboratory<sup>70</sup> and theoretical<sup>71</sup> studies have shown that the major scattering feature under these conditions is the vertical *stalk* that emerges shortly after drop impact. Moreover, these studies suggest that the V-polarized returns from raindrop splashes should be only mildly sensitive to the rain rate, while the H-polarized returns should show a strong dependence on both the rain rate and the drop-size distribution. Something of this behavior may be seen in the data in Figure 15.17. Open ocean measurements at K<sub>u</sub> band and at much higher grazing angles<sup>72</sup> show sufficient variability with wind speed, rain rate, and grazing angle to leave the uncertainties that opened this section largely unresolved.

In addition to scattering from the raindrop impacts, the distribution of raindrops in the volume of the atmosphere above the surface can have two additional effects on sea clutter—as an absorber/scatterer over the radar propagation path, which is well-understood, and as a mass-additive to the wind, affecting momentum transfer to the surface and thus the excitation of wind waves themselves, which is less well-understood.<sup>73</sup>

*Atmospheric Ducting.* Another topic in sea clutter that has been little explored is the role played by *propagation effects* within the atmospheric boundary layer lying over the sea surface. The effects of atmospheric absorption have been noted above in connection with millimeter-wave clutter, but at very low grazing angles, the ray paths joining the radar to the surface become very sensitive to refractive inhomogeneities in the atmospheric boundary layer. Over distances approaching and

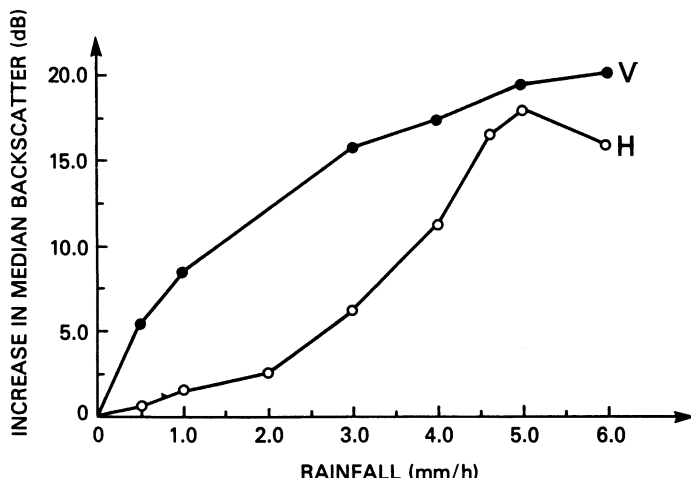


FIGURE 15.17 Sea clutter produced by rain splashes alone on a calm surface (20 dB corresponds to about  $\sigma^0 = -40$  dB) (from Hansen<sup>69</sup>)

beyond the conventional optical horizon, such perturbations could produce strong focus-defocus variations along the surface illumination profile<sup>74,75</sup> or a general rise in the local grazing angle.<sup>47</sup> Figure 15.18 gives an experimental example of the effect of *ducting* on very low-angle sea clutter.<sup>51</sup> The grazing angle given as the abscissa is actually a plot of inverse range, so the lifting of the cross section by ducting over an order-of-magnitude span of ranges is very likely due to a rise in the local grazing angle produced by refraction in the evaporative layer (first 10 meters or so above the surface).<sup>47</sup> Such effects should be suspected whenever the radar propagation path extends beyond the *optical* horizon.

*Shadowing.* The possibility of shadowing must be considered seriously whenever the sea is viewed at grazing angles smaller than the rms slope angle of the sea surface. Some examples were discussed earlier in connection with the behavior of sea clutter at low grazing angles in Figure 15.13. In fact, the sharp falloff of the *nonconducting* data in Figure 15.18 might be further evidence of the *threshold shadowing* mentioned earlier. However, the common idea of shadowing derives from the geometrical optics concept of a sharp transition between light and darkness. By considering the implications of *diffraction* at the wave peaks, it is possible to determine the domain of radar frequencies and wind speeds over which the concepts of geometrical optics may be applied. This was done in Wetzel,<sup>12</sup> where it is shown how diffraction, rather than geometrical shadowing, controls propagation into and out of the troughs of the waves under many of the usual frequencies and wind speeds encountered in practical radar operations at low grazing angles. For example, shadowing will take place at K<sub>a</sub> band for any winds above 15 kt, yet will hardly ever occur at L-band frequencies. Later analytical solutions based on numerical methods explored and expanded the idea of shadowing over the sea surface under highly idealized,<sup>76</sup> and more general<sup>77</sup> conditions.

*Surface Currents.* The most obvious effect of a current on sea clutter would be a shift in the peak of the doppler spectrum, analogous to the contribution of the 3% wind-drift current mentioned in connection with Eq. 15.11. Another effect is related to

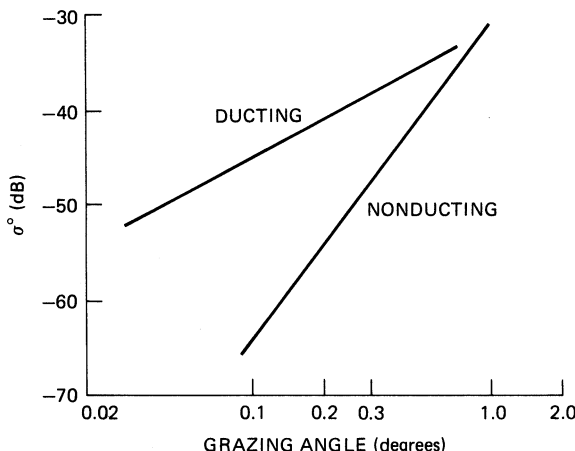


FIGURE 15.18 Effect of ducting on low-angle clutter; wind speed about 10 kt (after F. B. Dyer and N. C. Currie<sup>51</sup> © IEEE 1974)

the fact that the excitation of the surface-wave system depends on the local *apparent wind* at the surface, so there can be significant differences in waveheight according to whether the wind is blowing with or against the current. According to Eq. 15.6, waveheight is proportional to the square of the wind speed, so in the Gulf Stream, for example, with a current of 4 kt flowing north, a 15-kt northerly blowing against the current will raise a sea three times as high as a 15-kt southerly blowing with the current. Even with no wind, the presence of strong *current shears* can produce highly agitated surfaces. Shipboard observers have reported bands of roaring breakers passing by on an otherwise-smooth surface, presumably produced by powerful surface-current shears associated with large-amplitude internal waves.<sup>78</sup> In a more subtle way, modulated currents are held responsible for synthetic aperture radar (SAR) images that contain the expression of bottom topography produced by the Bernoulli Effect in shallow waters.<sup>79</sup> In each of the examples cited above, the current produces a change in the surface roughness, which can be expected to give rise to a change in sea clutter cross section.

*Contaminants.* The idea of pouring oil on troubled waters is a familiar one: the angry surface will smooth and subside. In another age, the survival-gear locker of every sailing ship would contain a bottle of oil to quiet the sea in a storm. Although the effectiveness of this procedure has always been somewhat controversial, there is no question that oil can produce a *slick* of smooth water at relatively low wind speeds. In fact, biological oils, produced by bacteria, algae, and plankton, can be found everywhere on the world's oceans and form natural slicks in those regions that combine the greatest oil concentration with the lowest wind speeds, e.g., close to continental shorelines.<sup>80</sup> Man-made contaminants can, of course, have the same effect. A layer of oil only one molecule thick will significantly affect the ability of the surface to support wave motions, but this layer must be continuous. The adjacent molecules then sense each other and form a film that is resistant to horizontal compression. The surface elasticity is changed, a type of longitudinal viscosity is introduced, and the surface becomes stabilized against the growth of short waves up to several inches in length.<sup>81,82</sup>

To the extent that radar sea clutter is produced by small-scale surface roughness (at grazing angles less than about 80°), the presence of oil on the surface should lead to a measurable decrease in clutter cross section. But, as noted above, the reduction of small wave motions requires the existence of a *continuous* monolayer; slick formation is a go-no-go process, and so slicks will tend to have relatively sharp boundaries. In operating the NRL 4FR system as a synthetic aperture radar to obtain images of the slicks produced by oil spills, Guinard found that the slicks were well defined, that it took very little oil to maintain a visible slick, that vertical polarization provided much greater contrast than did horizontal, and that the slicks were quenched by winds and currents.<sup>83</sup> Although signal strength was not recorded in this imaging experiment, later measurements at X and L bands by others<sup>84</sup> indicated that at the higher grazing angles (about 45°) the clutter reduction produced by the types of oil occurring in *natural* slicks was rather small, on the order of a percent. Since slicks are dispersed by the wind and associated wave action at wind speeds greater than about 10 kt, the effect of natural slicks on clutter may not be clear because they tend to occur in the regime of low wind speeds where the sea surface is already ill defined.

The celebrated *sun glitter* measurements by Cox and Munk<sup>85</sup> gave a quantitative measure of the effect of contaminants on the surface slopes in open water, showing that the wind-generated component of the rms slope of "oiled" waters is significantly

smaller than that of “clean” water. The heavy commercial oils used in their experiment were effective in suppressing small-scale waves over a range of wind speeds well beyond those which would normally disperse the lighter natural oils, so the effect of oil spills on sea clutter should be expected to extend to the higher wind speeds. In fact, at these higher wind speeds, the depression of radar backscatter by such oils at X and K<sub>a</sub> bands can reach 10 to 20 dB at intermediate grazing angles between 30° and 60°.<sup>86,87</sup>

## 15.4 THEORIES AND MODELS OF SEA CLUTTER

---

In addition to providing an intellectual basis for “understanding” sea clutter phenomena, a complete theory of sea clutter should ideally provide accurate *a priori* predictions of all aspects of clutter behavior under all possible environmental conditions. In spite of over 60 years of effort, the theory of sea clutter does neither of these tasks very well, as we will see in this section.

In the development of models of sea scatter based on physical theory, there are essentially two basic and distinct approaches. Historically, the first approach assumed sea scatter to have its origin in scattering *features*, or obstacles, actually present on or near the sea surface. Early scattering models included rain (to model spray),<sup>88</sup> smooth circular metallic disks,<sup>46,89</sup> arrays of semi-infinite planes,<sup>90</sup> and fields of hemispherical bosses,<sup>91</sup> to name a few. Obviously, the choice of these scattering obstacles related more to the preexistence of convenient scattering solutions for these shapes than to insights gained from observing the sea. Since then, feature models have sought greater reality by considering wedge shapes, as suggested by the sharp crests of Stokes waves observed on most natural water surfaces<sup>12,32,92,93</sup> and the shocks and plumes suggested by the properties of wave groups and the hydrodynamics of breaking waves.<sup>12,57</sup>

The other approach to theoretical modeling derives the scattered field from a global boundary-value problem (GBVP) in which the sea as a whole is considered a boundary surface whose corrugations are described by some kind of statistical process. An enormous literature is devoted to the theory of surface scatter from this point of view, stemming from the importance not only of radar sea scatter, but also radar ground scatter and sonar *reverberation* (the acoustic equivalent of radar clutter) from both the surface and the bottom of the sea. Because the GBVP approach leads to the analytical expression of the Bragg scattering hypothesis that has dominated the theory of sea scatter since the late 1960s, a brief explanation of some of the central ideas is included below.

**Theories Based on Global Boundary-Value Problems.** General formulations of the GBVP, though elegant, are of little practical value, and some kind of approximation is necessary to obtain useful quantitative results from them. The methods of approximation relate to the two methods of formulating the GBVP:

1. Small-amplitude approximations (sea waveheights much smaller than the radar wavelength) are used *ab initio* with Rayleigh’s hypothesis, in which the surface boundary conditions are employed to match an angular spectrum of outgoing plane waves to the incident field.<sup>94–96</sup>
2. A general integral formulation based on Green’s theorem is pursued either in a small-amplitude approximation<sup>6,97</sup> or under the assumptions of physical optics (surface curvatures much greater than the radar wavelength).<sup>98–100</sup>

In formulation 1, sometimes called the *small-perturbation method (SPM)* and associated most often with the work of Rice,<sup>94</sup> the surface displacements are assumed *everywhere* to be much smaller than the radar wavelength, so the method is directly applicable only to such cases as HF scattering with wavelengths of tens of meters, at low to intermediate wind speeds, and with waveheights of a few meters at most. The solution is in the form of a power series in the ratio of sea waveheight to radar wavelength, and it predicts the first-order Bragg lines and second-order spectral filling around the lines that were mentioned in the earlier section on HF sea clutter.

On the other hand, the various integral formulations referenced above usually begin with a very general expression for the fields scattered from the sea surface, which are squared and ensemble-averaged over realizations of the sea surface to provide the average power returned to the radar antenna, and then normalized to the illuminated area as in Eq. 15.7. Despite the generality of the initial formulations, most of the final expressions for  $\sigma^0$  either appear in, or can be put into, a form represented schematically by the following simplified one-dimensional expression (see Holiday et al.,<sup>10</sup> Bechmann and Spizzichino,<sup>99</sup> Fung and Pan,<sup>101</sup> and Valenzuela,<sup>102</sup> for example):

$$\sigma^0(\psi) = Ak^2 F_p(\psi) \int_{-\infty}^{\infty} dy e^{i2k_1 y} [e^{-4k_2^2 h^2 [1-C(y)]} - e^{-4k_2^2 h^2}] \quad (15.12)$$

where  $A$  is a constant;  $k_1 = k \cos \psi$  and  $k_2 = k \sin \psi$  where  $k$  is the radar wave-number ( $2\pi/\lambda$ );  $F_p(\psi)$  is a function of polarization  $p$ , grazing angle  $\psi$ , and the electrical properties of seawater;  $h$  is the rms sea waveheight; and  $C(y)$  is the surface correlation coefficient. Of course, the reduction of a complicated boundary-value problem to so simple a form requires assumptions about both the surface fields and the distribution of the sea heights (which is gaussian to a good approximation<sup>20</sup>). But while the SPM approach mentioned above requires the ratios  $h/\lambda$  to be small right at the start, GBVP theories derived from expressions resembling Eq. 15.12 have no *a priori* restrictions on surface heights.

The statistical properties of the sea surface enter through the correlation coefficient  $C(y)$  appearing under the integral sign in the exponential in the brackets, and by expanding this exponential in Eq. 15.12, it may be written

$$\sigma^0(\psi) = Ak^2 F_p(\psi) e^{-4k_2^2 h^2} \sum_{n=1}^{\infty} \frac{(4k_2^2)^n}{n!} W^{(n)}(2k_1) \quad (15.13)$$

where

$$W^{(n)}(2k_1) = \int_{-\infty}^{\infty} d\tau e^{i2k_1 \tau} [h^2 C(\tau)]^n \quad (15.14)$$

*Small-amplitude Approximation.* In the limit of small ratios of rms waveheight to radar wavelength or, more specifically,

$$2kh \ll 1 \quad (15.15)$$

only the first term in the series in Eq. 15.13 survives, and the cross section assumes the very simple form

$$\sigma^0(\psi) = 4\pi k^4 F'_p(\psi) W^{(1)}(2k \cos \psi) \quad (15.16)$$

where the constant  $A$  has been made explicit and  $F_p$  has absorbed a  $\sin^2$  term from the series.  $W^{(1)}$  is the Fourier transform of the surface correlation function, which makes it the sea wavenumber spectrum (discussed in Section 15.2) evaluated at twice the (surface-projected) radar wavenumber, which defines a *Bragg (or half-wavelength resonance)*. Except possibly for the details of the angle factor  $F_p$ , Eq. 15.16 is equivalent to the result obtained by the SPM discussed above, and although it is sometimes felt that its derivation from a surface integral provides some potential for greater generalization, it carries with it all of the same restrictions.

Before proceeding further, it is instructive to look a little more closely at the implications of the mathematical expressions in these formulations. Note that in Eq. 15.12 the expression in the brackets under the integral is the only place at which the surface-wave properties of the sea appear. That is, the cross section is simply proportional to the Fourier transform of a sea-surface functional, so the radar acts as a filter tuned to the “spatial frequency”  $2k \cos \psi$ , extracting that line from the spectrum of whatever assortment of scatterers the sea surface functional expresses, whether they be long swell components, short-wavelength noise, localized scattering features, or a chaotic tumble of water balls. Only under quite special circumstances will there actually be an identifiable surface-wave at that “frequency” that would justify the term *Bragg resonance* in its original sense, which, after all, was a resonance in an ordered crystal lattice of discrete scatterers. Although authors often refer to “free Bragg waves,” such objects are found primarily among the *parasitic capillaries* referred to in Section 15.2 or among the *ring waves* propagating out from the impact of a falling drop. This raises a question about the meaning of such often-used terms as *Bragg wavelets*, *Bragg patches*, and so on, as if such things had a real existence outside of their emergence as an artifact of a filter operation. This confusion of concepts might be avoided by visualizing the radar as extracting the “Bragg line” from the spectral compositions of those surface features that contain a wave of length  $\lambda/2\cos \psi$  in their Fourier representation, independent of the existence of such a wave as a real object.

Nevertheless, this direct linear relation between radar cross section and the oceanographers’ descriptor of the sea surface has had a powerful influence on thinking about the physical origins of sea clutter. It is appealing in its simplicity, and it suggests a direct way both to predict radar clutter from measurements or forecasts of the sea spectrum and, inversely, to use radar backscatter measurements to provide remote sensing of the sea surface for oceanographic and meteorological applications—provided, of course, that it correctly describes this relationship.

Although Eq. 15.16 successfully predicts (to 1st-order) the clutter returns at HF frequencies, at *microwave* frequencies the small-waveheight assumption on which this model rests is violated on any real sea surface. The small-waveheight condition expressed by Eq. 15.15 means that at X band, for example, the maximum departure of the sea surface from a flat plane must be much smaller than 3 mm.

*Other Calculational Strategies.* Instead of expanding the exponential in the integrand of Eq. 15.12, it should be possible, at least in principle, to replace  $C(y)$  directly by the Fourier transform of  $W(K)$  (the inverse of Eq. 15.14 for  $n = 1$ ), thus providing a direct functional relationship between the radar cross section and the sea wave spectrum without the restrictions of a small-amplitude approximation. This cumbersome approach involves extensive computations even to obtain limited results in individual cases, as shown in work by Holliday et al.<sup>10</sup>

In another limiting case, the basic integral formulation of the GBVP is solved in the optical approximation (large  $k$ ), resulting in an expression commonly called the

*specular return*, because its origin may be traced to pieces of the surface that provide a reflection point for the incident wave.<sup>99,102</sup> This expression is written for a gaussian sea surface in the form

$$\sigma^0(\psi) = (|R|^2/s^2) \csc^4 \psi \exp[-\cot^2 \psi / s^2] \quad (15.17)$$

where  $s$  is the rms surface slope and  $R$  is the flat-surface reflection coefficient for normal incidence. This is the type of scattering alluded to in connection with the high grazing angle returns discussed in Section 15.3; the tendency of  $\sigma^0$  to level off for grazing angles close to 90° (see Figures 15.3 and 15.4) may be ascribed to this mechanism.

From what has been said thus far, it can be seen that strict analytical solutions via the GBVP approach appear to run into dead ends: intractable formal expressions in the form of Eq. 15.12, small-amplitude approximations in the form of Eq. 15.16 that make little sense for microwave scattering from real sea surfaces, or optical limits such as Eq. 15.17 that relate to the probability densities of specularly reflecting surface slopes. It appears, therefore, that the use of integral formulations in the practical solution of the sea clutter problem at microwave frequencies will require something more.

*Composite-Surface Hypotheses.* Since it is not clear how to extend straightforward GBVP solutions beyond the limiting approximations described above, a heuristic model was developed that viewed the sea as a carpet of Bragg scattering “wavelets” modulated by the motions of the larger waves on the surface.<sup>102–104</sup> This *composite surface model* is often referred to as the *two-scale model*, in which it is imagined that the surface-wave spectrum can somehow be separated into two parts, one containing low-amplitude “Bragg scattering wavelets” whose integrated rms waveheight satisfies the conditions of Eq. 15.16 and another that contains only the longer waves that tilt and stretch and otherwise modulate the Bragg waves, affecting the Bragg scatterers through a *modulation transfer function*,<sup>105</sup> as well as providing a specular component resembling Eq. 15.17. Other assumptions include that (1) the correlation lengths of the short Bragg waves be long enough that a resonant interaction is possible, but short enough that adjacent areas on the surface contribute to the total signal in random phase (note how “Bragg waves” are viewed here as physical objects); and (2) the long waves that tilt and modulate the short waves have radii of curvature sufficiently large that the curvature over the correlation length of the “Bragg patches” is small in some sense. In its simplest and most commonly used “tilt” form, it interprets  $\sigma^0(\psi)$  in Eq. 15.16) as the cross section of a patch with *local* grazing angle  $\psi = \sigma^0 + \alpha$ , where  $\alpha$  is the local wave slope and  $\psi_0$  is the mean grazing angle. For the simple one-dimensional case, this quantity is averaged over the sea slope angle distribution  $p(\alpha)$ , yielding

$$\bar{\sigma}^0(\psi) = \int_{-\infty}^{\infty} \sigma^0(\psi_0 + \alpha) p(\alpha) d\alpha \quad (15.18)$$

For a more general two-dimensional sea, the local grazing angle is a function of the slopes in and normal to the plane of incidence, so for each polarization  $p$ , the angle function  $F_p(\psi)$  in  $\sigma^0(\psi)$  becomes a complex mixture of the angle functions of both polarizations. Plant<sup>104</sup> provides a comprehensive discussion of this model. Extensions of this model into what might be called a *three-scale model* are guided by the same ideas that led to the *two-scale model*.<sup>72,106</sup> An additional ad hoc spectral partition is introduced between the longest and shortest wave components of the sea spectrum, but this produced only modest improvement.<sup>106</sup>

Although such composite-surface models may leave the impression that they have emerged as a rigorous product of an integral formulation of the GBVP, it is clear that they are not really scattering *theories*, but instead scattering *pictures* assembled from a group of more or less plausible assumptions. But with the failure of the more formal GBVP theories to provide a general framework for predicting and understanding sea clutter, these models have become the basis for most analytical approaches to microwave scattering from the sea.

Figure 15.19 compares a sample of NRL 4FR data taken at high wind speeds ( $> 22$  kn) with the predictions of the pure SPM Bragg model (in the form of Eq. 15.16) for V-polarization and the *two-scale model* (in the form of Eq. 15.18) for H-polarization. The wave spectrum used was the Phillips spectrum given in Eq. 15.4. Historically, comparisons of this type have been used often to provide support for the Bragg scattering hypothesis,<sup>102,104</sup> and the agreement often looks good, especially for vertical polarization at the higher wind speeds. Yet why this is so remains a puzzling curiosity. In this example, the wind speeds are high so the sea will be rough, but it was noted above that the SPM approximation used in Figure 15.19 requires waveheights much less than a centimeter, so this approximation is totally invalid for these data. Moreover, the Phillips spectrum was used as the sea surface spectrum, but there is no evidence that this spectrum holds down to the required capillary wavelength of about 1.5 cm. In fact, the nature of the sea spectrum in this range remains uncertain and has been referred to as “one of the most exciting unsolved problems of the sea surface.”<sup>16</sup> The primary effect of the *two-scale model* is simply to raise the inapplicable SPM values for H-polarization, which are dropping sharply with grazing angle, by including higher local angles via Eq. 15.18. There would be little sensible effect on the more constant vertical returns. Finally, the polarization differences themselves have been shown to derive entirely from the behavior of the reflection coefficients at the underlying surface (see, for example, Wright<sup>6</sup> and Wetzel<sup>12</sup>), and so are not an intrinsic part of the Bragg hypothesis and would apply to *any* small perturbation on the surface. Nevertheless, agreement between measurement and prediction of the type illustrated in Figure 15.19

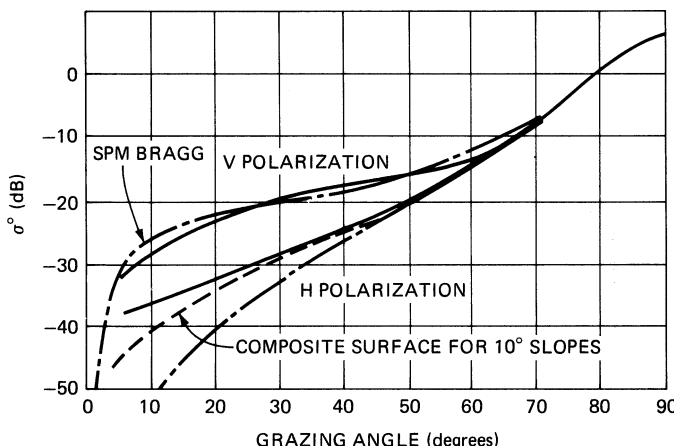


**FIGURE 15.19** Comparison of the predictions of the Bragg hypothesis with NRL 4FR data (heavy lines) for higher wind speeds ( $> 22$  kt): dash-dotted lines, SPM Bragg; dashed line, two-scale model for H-polarization only, assuming  $10^\circ$  mean sea slopes (after Valenzuela<sup>102</sup>)

has kept alive credibility in the Bragg scattering hypothesis in spite of the clear violations of conditions and nonsequiturs noted above, as well as the lack of a proper theory argued from first principles.

The failure of this model to account for sea spikes and other non-Rayleigh returns noted in Section 15.3 has led to an augmentation of the two-scale composite surface to include breaking waves, a presumed source of these returns. One of the latest of these *two-scale-plus* models may be found in Kudryavtsev et al.,<sup>107,108</sup> where breaking-wave effects are incorporated analytically through the Phillips expression<sup>23</sup> for the density of breaking fronts as a function of wind speed (the parameter  $\Lambda(c)$  noted in Section 15.2), with the scattering behavior based on Wetzel's plume model (see "Scattering by Surface Features"). The result is a significant improvement in sea scatter predictions, emphasizing the importance of breaking in the scattering scene. An example of this improvement is shown in Figure 15.20, where experimental data for the *polarization ratio* relative to wind direction was obtained from the Polrad96 program.<sup>107</sup> One of the major claims for Bragg models has been their apparent ability to agree loosely with the observed polarization ratios of sea clutter returns, and in Figure 15.20, as in Figure 15.19, the data were compared to the predictions of the SPM (pure) Bragg model and the two-scale model, while adding the *two-scale-plus* model, which incorporates the effects of breaking waves. In this case, the Bragg model and the two-scale model derived from it clearly fail to describe the observed behavior of the polarization ratio, while the inclusion of breaking waves (full model) provides a surprisingly faithful reproduction of the data, even at the high grazing angle of 50°. The X-band data illustrated previously in Figure 15.10a,b can also be shown to corroborate the predictions of this model for a similar wind speed and grazing angle, thus further supporting the suspicion that breaking-wave events will contribute importantly to sea clutter over *most* of the "rough surface" regime of grazing angles at these wind speeds.

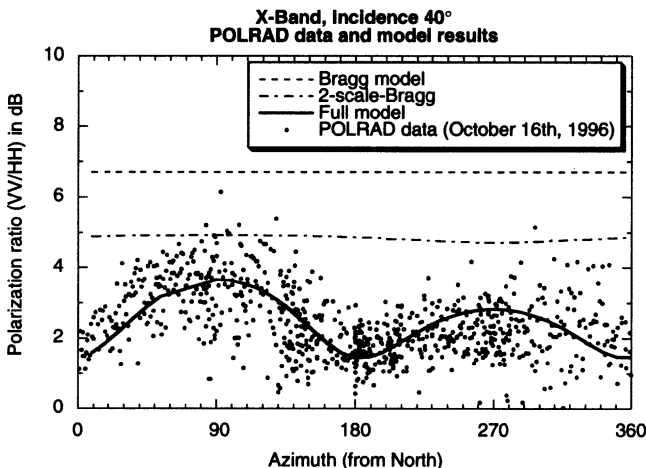


**FIGURE 15.20** Polarization ratio versus wind direction for X-band radar at 50° grazing angle and wind about 20 kt. Points: experimental data from Polrad96 experiment; dashed line: pure SPM Bragg; dashed-dotted line: two-scale Bragg; solid line: two-scale-plus model including breaking waves (after Kudryavtsev et al.<sup>107</sup>) © The American Geophysical Union 2003)

**Scattering by Surface Features.** A breaking wave, with plumes of water cascading down its face and perhaps a halo of spray above, is only one of the rich assortment of scattering elements appearing on the sea surface—including wedges, cusps, microbreakers, hydraulic shocks, patches of turbulence, and gravity-capillary waves (both wind-driven and parasitic)—any or all of which could contribute to the scattered clutter signal.

For example, the common Stokes wave<sup>20</sup> has a quasi-trochoidal structure that resembles a wedge on the surface, so wedge scatter might describe an important aspect of sea clutter.<sup>11,12,92,93</sup> The scattering model is usually some variant of the familiar *geometrical theory of diffraction* (GTD),<sup>109</sup> which is strictly applicable to the backscatter problem only when the edge of the wedge is normal to the plane of incidence. Nevertheless, the cross section predictions at the lower grazing angles for both polarizations show trends similar to the predictions of the Bragg or composite-surface models.<sup>93</sup>

One major problem with all models based on scattering feature simulations is the lack of reliable information about the shapes, sizes, orientations, speeds, lifetimes and statistics of the features themselves. Thus, although there is often guidance from either observation or theory, the predictions of such models will be based on uncertain assumptions about these crucial parameters. As an example, water surface stability arguments prevent the interior angle of a sharpening wave crest from falling below 120°, which then becomes a convenient measure of the wedge angle in wedge-scattering models. In Figure 15.21, the overall scale of wedge scattering as calculated by the GTD was adjusted to locate the cluster of cross sections at the level of the experimental values. Wedges appear to model the qualitative behavior with both polarizations fairly well at the lower grazing angles.

Figure 15.21 also includes two additional simple scattering models for comparison. Lambert's law, mentioned in connection with Figure 15.9a,b, expresses the cross section in the form  $\sigma^0 = A \sin^2 \psi$ , where  $A$  is the *surface albedo*. Choosing  $A = -13$  dB (a reasonable value for microwave frequencies) gives a fairly good match to the vertically polarized returns over a wide range of grazing angles. The *facet* model, expressed

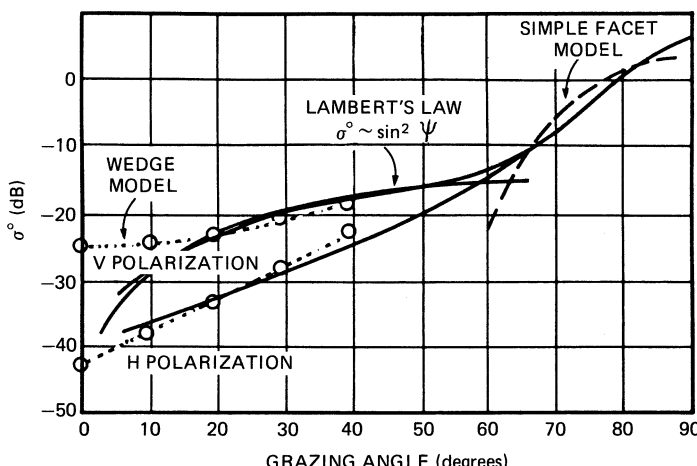


**FIGURE 15.21** Comparison of several ad hoc feature models with NRL 4FR data (data the same as shown in Figure 15.19)

by Eq. 15.17 and thought to describe clutter at the higher grazing angles, is shown for 20 kt seas.<sup>102</sup> The general behavior described by these two models seems to agree about as well as any other, although they too must employ arbitrary assumptions to obtain reasonable fits to the data, so the significance of this agreement is difficult to assess. However, one might deduce from Figure 15.21 that sharp things (like wedges) dominate the clutter at small grazing angles, flat things (like facets) at large angles, and generally rough things at the intermediate angles.

The theory of scattering from breaking waves referenced in connection with Figure 15.20 was originally motivated by an attempt to explain the complex behavior of sea spikes at low grazing angles observed by Lewis and Olin.<sup>40</sup> This theory was based on the *plume model* of the most common *spilling* breaker, in which a water plume is emitted at the spilling crest and moves down the front face;<sup>110</sup> the scattering behavior was supplied by multipath illumination involving reflections from the face of the wave.<sup>57</sup> The elaboration of this model explained much of the complex behavior of the observed sea spikes; however, like all other models based on scattering features, it was necessary to make assumptions about the sizes, shapes, and lifetimes of the scattering plumes. These parameters were all inferred from observation of real sea surfaces, and the resulting predictions were surprisingly good. Additionally, its success in the *two-scale-plus* model mentioned above provides further credibility.

Although scattering features have been introduced mainly in connection with low-grazing-angle sea clutter (see Wetzel<sup>12</sup> for a detailed discussion), there is evidence, as noted above, to believe that feature scattering operates at all grazing angles. Considering the failure of scattering theories formulated as a GBVP to provide any predictions beyond those in certain limiting-case approximations and the precarious nature of the logical infrastructure of the Bragg hypothesis in microwave scattering from a natural sea, it is quite possible that further careful consideration of the actual scattering features present on the sea surface will improve our understanding of sea clutter in the future.

**Implications of Surface Geometry.** The approximations to the GBVP discussed above were all formulated in the frequency domain, but a time-domain model for sea scatter points to a possible general surface-geometric origin for the surface returns.<sup>13,110</sup> The model introduces the idea that the basic scattering elements of a surface are localized at points of *high surface curvature*, as at the sharp tips of small Stokes waves or at the corner of a plume intersecting the front face of a breaking wave. Using a  $\delta$ -function as a probing pulse, an approximate expression for the scattering cross section was found as a function of surface curvature  $\mathcal{C}(\mathbf{r}(t_o))$ , where  $t_o$  is the round-trip time from the radar to a point  $\mathbf{r}(t_o)$  on the surface

$$\sigma(t_o) = B(\psi, s, t_o) \mathcal{C}^2(ct_o / 2\cos\psi) \quad (15.19)$$

with  $B$  a complicated trigonometric function of grazing angle  $\psi$ , surface slope  $s$ , and  $t_o$ . The factor  $B$  peaks at points of specular reflection, so Eq. 15.19 expresses the effects of specular glints as well as sharp curvatures. Although the original theory<sup>13</sup> is based on a physical optics formulation for a scalar field (see Sangston<sup>111</sup> for the vector form), some support for its implications can be gained from a plot of the square of surface curvature over a real sea surface. Figure 15.22a shows the *surface slope* measured over a short segment of surface in the Gulf Stream,<sup>112</sup> with the corresponding *curvature-squared* profile below. The clutter cross-section defined for this profile

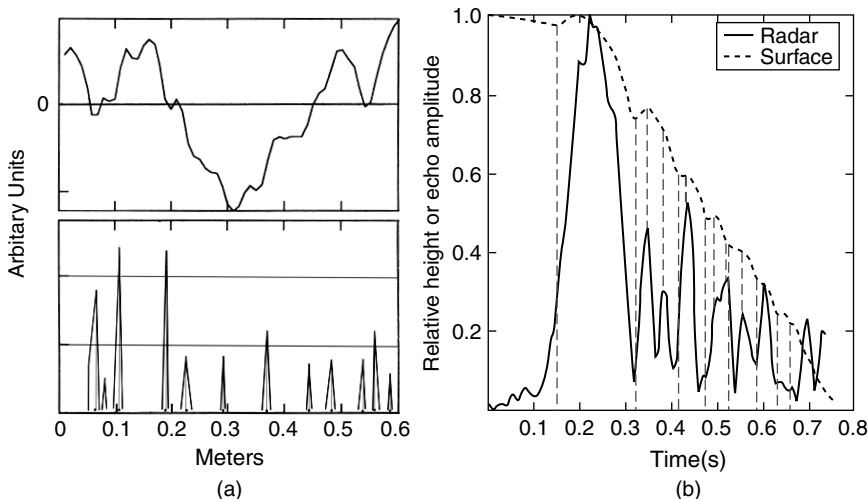


**FIGURE 15.22** (a) Measured slope (top curve) over a sampled surface in the Gulf Stream,<sup>112</sup> with the corresponding square of the surface curvature below; (b) Wave-tank measurement of radar scattering from an evolving breaking wave, correlated with wave surface height variations (from M. A. Sletten and J. C. West<sup>114</sup> © The American Geophysical Union 2003)

by Eq. 15.19 clearly bears a resemblance to some of the high resolution returns shown in Figure 15.11. Moreover, these spiky returns are correlated with just the kind of surface bumps and wrinkles and slope discontinuities that have been identified as sources of sea spikes in laboratory tank measurements.<sup>11,113,114</sup> An example is shown in Figure 15.22b, where an ultra-high-resolution radar looks at the return from a breaking wave whose surface is evolving as plotted above the radar signal. We see that the spikes appear at the points of maximum surface curvature, although the large signal peak is probably a specular reflection from the initial breaking front.

It is often overlooked that the presumed origin of sea scatter is suggested by the kind of measuring instrument being used, which in turn determines the most appropriate theoretical basis—i.e., the “theory of the experiment.” If you go to sea with a CW radar—an “averaging wave spectrometer”—you will be selecting a spectral line by long integration times and interpret the origin as a wave effect, namely a “Bragg resonance.” On the other hand, if you use a high resolution probe—a radar microscope—the clutter scene will be populated by highly localized scattering events, or *sea spikes*, isolated by a short-pulse, wide-bandwidth signal. In this case, the most appropriate “theory of the experiment” is the time-domain formalism described above.

Other ways of viewing sea clutter in terms of surface geometry characterize the sea and the clutter as fractal processes,<sup>115</sup> or seek parameters describing its complexity by defining a “strange attractor.”<sup>116</sup> Unfortunately, these studies do not seem to contain any useful insights into the physical scattering processes at the surface, except, perhaps, to conclude that sea clutter arises from multiple sources, which we already know. On the other hand, the identification of changes in the characteristic *measures* of these processes (e.g., fractal dimension and embedding dimension) have been proposed as a way to identify the presence of targets in clutter.

**Numerical Methods.** With rapid increases in computer speed, it has become practical to solve certain scattering problems by numerical methods, thereby sidestepping the introduction of the approximations required by the analytical solutions described above. In surface scattering, particularly for the continuous sea surface, the method of choice appears to be some variant of the Method of Moments.<sup>117</sup> An exact integral equation for the *surface currents* excited by an illuminating field is solved numerically over a grid of points, where the flexibility and accuracy of the solution depends, essentially, on the grid spacing, the size of the surface features compared to the illuminating wavelength, the extent of the surface over which the grid is laid, and the efficiency of the computing algorithms used in what are extensive calculations. Once found for an ensemble of surface realizations, these currents can be used in a scattering integral over each of the surfaces to generate an ensemble of *scattered fields*, which are finally averaged into a surface scattering cross section.<sup>118</sup> Although these methods are often viewed as the “gold standard” for doing scattering calculations, their complexity and difficulty generally restrict their application to idealized or laboratory surface structures, where they simply confirm that Maxwell’s equations continue to be verified in scattering experiments. Nevertheless, such numerical simulations can be informative in identifying the source of particular scattering events, such as sea spikes, along with their dependence on such radar parameters as grazing angle, polarization, and frequency.<sup>119,120</sup>

**Role of Laboratory Studies.** The sea surface is a natural system controlled by the laws of hydrodynamics. But so is a bowl of soup or a tank of water or a rushing stream—all of which might share certain behaviors with a sea surface, while presenting a venue much more amenable to the comfortable investigation of scattering phenomenology. While there is the obvious matter of *scale*, one might entertain the notion that what is found to hold in the small compass of a laboratory wave tank might transfer with little alteration to the open ocean. But this certainly cannot be true; the sea surface is structured by large-scale wind systems, impossible to duplicate under laboratory conditions. Therefore, the laboratory is used almost exclusively to study in detail how an electromagnetic wave interacts with some restricted and well-controlled aspect of surface phenomenology that is thought to be involved in the open sea.

There is a vast literature extending over almost 45 years reporting a wide variety of laboratory experiments on microwave scattering from a disturbed water surface. The earliest appear to be careful small-scale experiments in the mid-1960s to confirm the existence of Bragg scatter at centimeter wavelengths,<sup>6</sup> while at the other end of the experimental scale, the chaos of a full-scale breaker was simulated by submerging a hydrofoil across a 7 meter wide circulating water channel driven by 1.5 megawatts of turbine power.<sup>121</sup> But most laboratory experiments are more modest, involving a long wave tank, perhaps a meter or two across, with the wave system produced by either a controlled wind or a programmed wavemaker.

To illustrate a few of the experiments and their results: Kwoh and Lake<sup>11</sup> measured X-band returns from gentle breaking waves in a wave tank and found that specular and curvature scattering appeared to dominate over Bragg scattering for such surfaces. Keller et al.,<sup>122</sup> measured X-band returns and surface spectrum simultaneously in a wave tank and found Bragg-based theories might have credence at intermediate grazing angles and strong winds, but were unable to account for scattering behavior under other conditions. Sletten and West<sup>113,114</sup> made a two-pronged approach to breaking wave scatter, constructing a metallic model of a breaking wave, comparing its

scattering properties with numerical calculations, and then going to the wave tank to verify the scattering behavior for real water waves. Ericson et al.<sup>123</sup> generated a stationary breaker in a small flow tunnel and compared its scattering properties with a specular point calculation. Coakley et al.<sup>121</sup> set up a hydrofoil in a powerful water channel, generating a large breaking wave front that produced radar returns consistent with Lambert's Law, along with the polarization ratios implied by multipath reflections from the undisturbed front face. These investigators, along with many others, have been exploring radar scattering from water surfaces in ways that can be expected to contribute significantly to our growing understanding of sea clutter.

## 15.5 SUMMARY AND CONCLUSIONS

---

In the early days of radar, the importance of knowing the sea clutter environment led to many experiments under a variety of conditions. Variations in quality and completeness of ground truth, calibration of the equipment, and the experimenter's experience led to results that often showed considerable inconsistency and suggested clutter behavior that was sometimes more a function of the vagaries of the experiment than of the physics of the clutter. As data of increasingly better quality accumulated, it might have been expected that the behavior of sea clutter would be established with increasing confidence. This has not always been so, leaving our general knowledge about sea clutter to be summarized roughly as follows: For the higher 50% of wind speeds encountered over the world's oceans (greater than about 15 kt), microwave sea clutter at intermediate to high grazing angles has little dependence on frequency, and the effects of wind speed are uncertain, seeming to depend on polarization, wind direction, and grazing angle in often confusing ways. Yet various empirical descriptions and statistical characterizations are available that allow much of the useful sea clutter regime to be described in ways that can be of practical value to the radar community, provided that some care is taken in defining and observing the pertinent parameters. However, there are major areas of uncertainty present at any wind speed, whenever the grazing angle goes below a few degrees and the surface illumination begins to feel the effects of refraction and diffraction, and at *any* grazing angle, whenever the wind speed is less than about 10 kt, where peculiarities and uncertainties in the generation of surface roughness begin to emerge most strongly. At the low grazing angles encountered in maritime radar operations, sea clutter becomes spiky and intermittent, requiring special attention to signal processing and the interpretation of the radar signal. Moreover, features of the sea environment such as rain, currents, slicks, and refractive anomalies can confuse the reliable separation of target returns from clutter artifacts.

The question of microwave sea clutter theory remains unsettled. The most popular model, the two-scale Bragg model, is actually an assemblage of assumptions supported by circumstantial evidence; there is still no clear reason why it should work when it does. In fact, there is increasing evidence from both the tank and the open ocean that this model fails to account for many aspects of measured sea scatter behavior. Augmenting it with a term expressing the effect of breaking waves in active seas has improved predictions, but still perpetuates the ad hoc character of composite-surface models. Theories based on scattering by surface features have begun to show promise, and at least one of these features—the breaking wave at various scales, macro to micro—is increasingly recognized as an important contributor to

sea clutter for low grazing angles and short pulses in particular. The major problem of characterizing these features in a manner useful to quantitative predictions is still being addressed. Perhaps the expression of the scattering properties of the surface in terms of an intrinsic surface property like its fine-scale curvature might introduce an organizing principle for the many bits and pieces that presently make up the theory of sea scatter.

In the last edition of this Handbook (1990), the final statement in this chapter was "It will be interesting to see what progress will have been made in the theory of sea clutter by the publication of the next edition of this handbook." It appears that the answer is—not much. But there is some evidence that the theory of sea scatter is gradually being freed from the paralyzing monotheism of Bragg scatter, so there is hope for the future.

## REFERENCES

---

1. D. E. Kerr, *Propagation of Short Radio Waves*, New York: McGraw-Hill Book Company, 1951.
2. M. I. Skolnik, *Introduction to Radar Systems*, 3rd Ed., New York: McGraw-Hill Book Company, 2001.
3. F. E. Nathanson, *Radar Design Principles*, 2nd Ed., New York: McGraw-Hill Book Company, 1991.
4. M. W. Long, *Radar Reflectivity of Land and Sea*, 3rd Ed., Norwood, MA: Artech House, 2001.
5. D. Crombie, "Doppler spectrum of sea echo at 13.56 Mc/s," *Nature*, vol. 175, pp. 681–683, 1955.
6. J. W. Wright, "A new model for sea clutter," *IEEE Trans.*, vol. AP-16, pp. 217–223, 1968.
7. F. G. Bass, I. M. Fuks, A. I. Kalmykov, I. E. Ostruvsky, and A. D. Rosenberg, "Very high frequency radio wave scattering by a disturbed sea surface," *IEEE Trans.*, vol. AP-16, pp. 554–568, 1968.
8. D. Barrick and Q. Peake, "A review of scattering from surfaces with different roughness scales," *Radio Sci.*, vol. 3, pp. 865–868, 1968.
9. D. Atlas, R. C. Beal, R. A. Brown, P. De Mey, R. K. Moore, C. G. Rapley, and C. T. Swift, "Problems and future directions in remote sensing of the oceans and troposphere: a workshop report," *J. Geophys. Res.*, vol. 9(C2), pp. 2525–2548, 1986.
10. D. Holiday, G. St-Cyr, and N. E. Woods, "A radar ocean imaging model for small to moderate incidence angles," *Int. J. Remote Sensing*, vol. 7, pp. 1809–1834, 1986.
11. D. S. Kwoh and B. M. Lake, "A deterministic, coherent, and dual-polarized laboratory study of microwave backscattering from water waves, part 1: Short gravity waves without wind," *IEEE J. Oceanic Eng.*, vol. OE-9, pp. 291–308, 1984.
12. L. B. Wetzel, "Electromagnetic scattering from the sea at low grazing angles," in *Surface Waves and Fluxes: Current Theory and Remote Sensing*, chap. 12, G. L. Geernaert and W. J. Plant (eds.), Dordrecht, Netherland: Reidel, 1989.
13. L. B. Wetzel, "A time domain model for sea scatter," *Radio Sci.*, vol. 28, no. 2, pp. 139–150, March–April 1993.
14. D. Middleton and H. Mellin, "Wind-generated solutions, A potentially significant mechanism in ocean surface wave generation and wave scattering," *IEEE J. Oceanic Eng.*, vol. OE-10, pp. 471–476, 1985.
15. S. Tang and O. H. Shemdin, "Measurement of high-frequency waves using a wave follower," *J. Geophys. Res.*, vol. 88, pp. 9832–9840, 1983.
16. W. J. Pierson and L. Moskowitz, "A proposed spectral form for fully developed seas based on the similarity theory of S. A. Kitaigorodskii," *J. Geophys. Res.*, vol. 69, pp. 5181–5190, 1964.

17. O. M. Phillips, "Spectral and statistical properties of the equilibrium range in wind-generated gravity waves," *J. Fluid Mech.*, vol. 156, pp. 505–531, July 1985.
18. W. J. Pierson, Jr. and M. A. Donelan, "Radar scattering and equilibrium ranges in wind-generated waves with application to scatterometry," *J. Geophys. Res.*, vol. 91(C5), pp. 4971–5029, 1987.
19. S. A. Kitaigorodskii, "On the theory of the equilibrium range in the spectrum of wind-generated gravity waves," *J. Phys. Oceanogr.*, vol. 13, pp. 816–827, 1983.
20. B. Kinsman, *Wind Waves*, Englewood Cliffs, NJ: Prentice-Hall, 1965.
21. O. M. Phillips, F. L. Posner, and J. P. Hansen, "High range resolution radar measurements of the speed distribution of breaking events in wind generated waves: Surface impulse and wave energy dissipation rates," *J. Phys. Oceanogr.*, vol. 21, 450, 2001.
22. J. Wu, "Variations of whitecap coverage with wind stress and water temperature," *J. Phys. Oceanogr.*, vol. 18, pp. 1448–1453, October 1988.
23. O. M. Phillips, "Radar returns from the sea surface–Bragg scattering and breaking waves," *J. Phys. Oceanogr.*, vol. 18, pp. 1063–1074, 1988.
24. W. P. Plant, "A new interpretation of sea surface slope probability density functions," *J. Geophys. Res.*, vol. 108, no. C9, p. 3295, 2003.
25. J. C. Daley, J. T. Ransone, J. A. Burkett, and J. R. Duncan, "Sea clutter measurements on four frequencies," Naval Res. Lab. Rept. 6806, November 1968.
26. G. R. Valenzuela and R. Laing, "On the statistics of sea clutter," Naval Res. Lab. Rept. 7349, December 1971.
27. N. W. Guinard, J. T. Ransone, Jr., and J. C. Daley, "Variation of the NRCS of the sea with increasing roughness," *J. Geophys. Res.*, vol. 76, pp. 1525–1538, 1971.
28. J. C. Daley, "Wind dependence of radar sea return," *J. Geophys. Res.*, vol. 78, pp. 7823–7833, 1973.
29. K. D. Ward, C. J. Baker, and S. Watts, "Maritime surveillance radar Part 1: Radar scattering from the ocean surface," *IEE Proc.*, vol. 137, Pt F, no. 2, April 1990.
30. S. Watts, K. D. Ward, and R.T. A. Tough, "The physics and modeling of discrete spikes in radar sea clutter," presented at 2005 IEEE International Radar Conference, 2005.
31. H. Masuko, K. Okamoto, M. Shimada, and S. Niwa, "Measurement of microwave backscattering signatures of the ocean surface using X band and  $K_a$  band airborne scatterometers," *J. Geophys. Res.*, vol. 91(C11), pp. 13065–13083, 1986.
32. A. I. Kalmykov and V. V. Pustovoytenko, "On Polarization features of radio signals scattered from the sea surface at small grazing angles," *J. Geophys. Res.*, vol. 81, pp. 1960–1964, 1976.
33. I. Katz and L. M. Spterne, "Polarization and depression angle dependence of radar terrain return," *J. Res. Natl. Bur. Stand., Sec. D.* vol. 64-D, pp. 483–486, 1960.
34. F. Feindt, V. Wismann, W. Alpers, and W. C. Keller, "Airborne measurements of the ocean radar cross section at 5.3 GHz as a function of wind speed," *Radio Sci.*, vol. 21, pp. 845–856, 1986.
35. L. C. Schroeder, P. R. Schaffner, J. L. Mitchell, and W. L. Jones, "AAFE RADSCAT 13.9-GHz measurements and analysis: Wind-speed signature of the ocean," *IEEE J. Oceanic Eng.*, vol. OE-10, pp. 346–357, 1985.
36. G. P. de Loor and P. Hoogeboom, "Radar backscatter measurements from Platform Noordwijk in the North Sea," *IEEE J. Oceanic Eng.*, vol. OE-7, pp. 15–20, January 1982.
37. A. H. Chaudhry and R. K. Moore, "Tower-based backscatter measurements of the sea," *IEEE J. Oceanic Eng.*, vol. OE-9, pp. 309–316, December 1984.
38. F. T. Ulaby, R. K. Moore, and A. K. Fung, *Microwave Remote Sensing, Active and Passive*, Vol. III, Reading, MA: Addison-Wesley Publishing Company, 1986, Sec. 20.2.
39. B. Spaulding, D. Horton, and P. Huong, "Wind Aspect Factor in Sea Clutter Modeling," presented at 2005 IEEE International Radar Conference, 2005.
40. B. L. Lewis and I. D. Olin, "Experimental study and theoretical model of high-resolution backscatter from the sea," *Radio Sci.*, vol. 15, pp. 815–826, 1980.
41. J. P. Hansen and V. F. Cavalieri, "High resolution radar sea scatter, experimental observations and discriminants," Naval Research Laboratory Report No. 8557, 1982.

42. D. Trizna, "Measurement and interpretation of North Atlantic Ocean Marine Radar Sea Scatter," Naval Res. Lab. Rept. 9099, May 1988.
43. P. Beckmann, *Probability in Communication Engineering*, New York: Harcourt, Brace and World, Inc., 1967, Sect. 6.2.
44. G. V. Trunk, "Radar properties of non-Rayleigh sea clutter," *IEEE Trans.*, vol. AES-8, pp. 196–204, 1972.
45. P. H. Y. Lee, J. D. Barter, K. L. Beach, C. L. Hindman, B. M. Lake, H. Rungaldier, J. C. Shelton, A. B. Williams, R. Yee, and H. C. Yuen, "X band microwave scattering from ocean waves," *J. Geophys. Res.*, vol. 100, no. C2, pp. 2591–2611, February 1995.
46. M. Katzin, "On the mechanisms of radar sea clutter," *Proc. IRE*, vol. 45, pp. 44–45, January 1957.
47. L. B. Wetzel, "A model for sea backscatter intermittency at extreme grazing angles," *Radio Sci.*, vol. 12, pp. 749–756, 1977.
48. I. M. Hunter and T. B. A. Senior, "Experimental studies of sea surface effects on low angle radars," *Proc. IEE*, vol. 113, pp. 1731–1740, 1966.
49. H. Sittrop, "X- and K<sub>u</sub>-band radar backscatter characteristics of sea clutter," in *Proc. URSI Commission II Specialist Meeting on Microwave Scattering from the Earth*, E. Schanda (ed.), Bern, 1974.
50. B. G. Smith, "Geometrical shadowing of the random rough surface," *IEEE Trans.*, vol. AP-15, pp. 668–671, 1967.
51. F. B. Dyer and N. C. Currie, "Some comments on the characterization of radar sea echo," in *Dig. Int. IEEE Symp. Antennas Propagat.*, July 10–12, 1974.
52. D. E. Barrick, J. M. Headrick, R. W. Bogle, and D. D. Crombie, "Sea backscatter at HF: Interpretation and utilization of the echo," *Proc. IEEE*, vol. 62, 1974.
53. C. C. Teague, G. L. Tyler, and R. H. Stewart, "Studies of the sea using HF radio scatter," *IEEE J. Oceanic Eng.*, vol. OE-2, pp. 12–19, 1977.
54. J. C. Wiltse, S. P. Schlesinger, and C. M. Johnson, "Back-scattering characteristics of the sea in the region from 10 to 50 KMC," *Proc. IRE*, vol. 45, pp. 220–228, 1957.
55. G. W. Ewell, M. M. Horst, and M. T. Tuley, "Predicting the performance of low-angle microwave search radars—Targets, sea clutter, and the detection process," *Proc. OCEANS 79*, pp. 373–378, 1979.
56. W. K. Rivers, "Low-angle radar sea return at 3-mm wavelength," Final Tech. Rept., Georgia Institute of Technology, Engineering Experiment Station, Contract N62269-70-C-0489, November 1970.
57. L. B. Wetzel, "On microwave scattering by breaking waves," in *Wave Dynamics and Radio Probing of the Ocean Surface*, Chap. 18, O. M. Phillips and K. Hasselmann (eds.), New York: Plenum Press, 1986, pp. 273–284.
58. B. L. Hicks, N. Knable, J. Kovaly, G. S. Newell, J. P. Ruina, and C. W. Sherwin, "The spectrum of X-band radiation backscattered from the sea surface," *J. Geophys. Res.*, vol. 65, pp. 825–837, 1960.
59. G. R. Valenzuela and R. Laing, "Study of doppler spectra of radar sea echo," *J. Geophys. Res.*, vol. 65, pp. 551–562, 1970.
60. V. W. Pidgeon, "Doppler dependence of sea return," *J. Geophys. Res.*, vol. 73, pp. 1333–1341, 1968.
61. Y. U. Mel'nicuk and A. A. Chernikov, "Spectra of radar signals from sea surface for different polarizations," *Izv. Atmos. Oceanic Phys.*, vol. 7, pp. 28–40, 1971.
62. J. W. Wright and W. C. Keller, "Doppler spectra in microwave scattering from wind waves," *Phys. Fluids*, vol. 14, pp. 466–474, 1971.
63. D. Trizna, "A model for doppler peak spectral shift for low grazing angle sea scatter," *IEEE J. Oceanic Eng.*, vol. OE-10, pp. 368–375, 1985.
64. P. H. Y. Lee, J. D. Barter, K. L. Beach, E. Caponi, C. L. Hindman, B. M. Lake, H. Rungaldier, and J. C. Shelton, "Power spectral lineshapes of microwave radiation backscattered from sea surfaces at small grazing angles," *IEE Proc.-Radar, Sonar Navig.*, vol. 142, no. 5, pp. 252–258, October 1995.
65. F. E. Nathanson, *loc cit*, Sec. 7.5.

66. W. C. Keller, W. J. Plant, and G. R. Valenzuela, "Observation of breaking ocean waves with coherent microwave radar," in *Wave Dynamics and Radio Probing of the Ocean Surface*, chap. 19, O. M. Phillips and K. Hasselmann (eds.), New York: Plenum Press, 1986, pp. 285–292.
67. R. K. Moore, Y. S. Yu, A. K. Fung, D. Kaneko, G. J. Dome, and R. E. Werp, "Preliminary study of rain effects on radar scattering from water surfaces," *IEEE J. Oceanic Eng.*, vol. OE-4, pp. 31–32, 1979.
68. R. F. Contreras, W. J. Plant, W. C. Keller, K. Hayes, and J. Nystuen, "Effects of rain on Ku band backscatter from the ocean," *J. Geophys. Res.*, vol. 108, no. C5, pp. 3165–3180, 2003.
69. J. P. Hansen, "High resolution radar backscatter from a rain disturbed sea surface," presented at ISNR-84 Rec., Tokyo, October 22–24, 1984.
70. J. P. Hansen, "A system for performing ultra high resolution backscatter measurements of splashes," in *Proc. Int. Microwave Theory & Techniques Symp.*, Baltimore, 1986.
71. L. B. Wetzel, "On the theory of electromagnetic scattering from a raindrop splash," *Radio Sci.*, vol. 25, No. 6, pp. 1183–1197, 1990.
72. R. Romeiser, A. Schmidt, and W. Alpers, "A three-scale composite surface model for the ocean wave-radar modulation transfer function," *J. Geophys. Res.*, vol. 99, pp. 9785–9801, 1994.
73. B. LeMehaute and T. Khangaonkar, "Dynamic interaction of intense rain with water waves," *J. Phys. Oceanogr.*, vol. 20, December 1990.
74. L. B. Wetzel, "On the origin of long-period features in low-angle sea backscatter," *Radio Sci.*, vol. 13, pp. 313–320, 1978.
75. P. Gerstoft, L. T. Rogers, W. S. Hodgkiss, and L. J. Wagner, "Refractivity estimation using multiple elevation angles," *IEEE J. of Oceanic Eng.*, vol. 28, no. 3, pp. 513–525, July 2003.
76. D. E. Barrick, "Near-grazing illumination and shadowing of rough surfaces," *Radio Sci.*, vol. 30, no. 3, pp. 563–580, May-June 1995.
77. J. M. Sturm and J. C. West, "Numerical study of shadowing in electromagnetic scattering from rough dielectric surfaces," *IEEE Trans. in Geosci. and Remote Sensing*, vol. 36, no. 5, September 1998.
78. R. B. Perry and G. R. Schimke, "Large-amplitude internal waves observed off the northwest coast of Sumatra," *J. Geophys. Res.*, vol. 70, pp. 2319–2324, 1965.
79. W. Alpers and I. Hennings, "A theory of the imaging mechanism of underwater bottom topography by real and synthetic aperture radar," *J. Geophys. Res.*, vol. 89, pp. 10529–10546, 1984.
80. W. Garrett, "Physicochemical effects of organic films at the sea surface and their role in the interpretation of remotely sensed imagery," in *ONRL Workshop Proc.—Role of Surfactant Films on the Interfacial Properties of the Sea Surface*, F. L. Herr and J. Williams (eds.), November 21, 1986, pp. 1–18.
81. H. Hühnerfuss, W. Alpers, W. D. Garrett, P. A. Lange, and S. Stolte, "Attenuation of capillary and gravity waves at sea by monomolecular organic surface films," *J. Geophys. Res.*, vol. 88, pp. 9809–9816, 1983.
82. J. C. Scott, "Surface films in oceanography," in *ONRL Workshop Proc.—Role of Surfactant Films on the Interfacial Properties of the Sea Surface*, F. L. Herr and J. Williams (eds.), November 21, 1986, pp. 19–40.
83. N. W. Guinard, "Radar detection of oil spills," presented at Joint Conf. Sensing of Environmental Pollutants, AIAA Pap. 71–1072, Palo Alto, CA, November 8–10, 1971.
84. H. Hühnerfuss, W. Alpers, A. Cross, W. D. Garrett, W. C. Keller, P. A. Lange, W. J. Plant, F. Schlude, and D. L. Schuler, "The modification of X and L band radar signals by monomolecular sea slicks," *J. Geophys. Res.*, vol. 88, pp. 9817–9822, 1983.
85. C. S. Cox and W. H. Munk, "Statistics of the sea surface derived from sun glitter," *J. Mar. Res.*, vol. 13, pp. 198–227, 1954.
86. W. Alpers and H. Hühnerfuss, "Radar signatures of oil films floating on the sea surface and the Marangoni effect," *J. Geophys. Res.*, vol. 93, pp. 3642–3648, April 15, 1988.
87. H. Masuko and H. Inomata, "Observations of artificial slicks by X and K<sub>a</sub> band airborne scatterometers," in *Proc. Int. Geoscience and Remote Sensing Symp. (IGARSS'88)*, Edinburgh, September 12–16, 1988, pp. 1089–1090. Published by Noordwijk, Netherlands: European Space Agency, ESTEC, 1988.

88. H. Goldstein, "Frequency dependence of the properties of sea echo," *Phys. Rev.*, vol. 70, pp. 938–946, 1946.
89. A. H. Schooley, "Some limiting cases of radar sea clutter noise," *Proc. IRE*, vol. 44, pp. 1043–1047, 1956.
90. W. S. Ament, "Forward and backscattering by certain rough surfaces," *Trans. IRE*, vol. AP-4, pp. 369–373, 1956.
91. V. Twersky, "On the scattering and reflection of electromagnetic waves by rough surfaces," *Trans. IRE*, vol. AP-5, pp. 81–90, 1957.
92. D. R. Lyzenga, A. L. Maffett, and R. A. Schuchman, "The contribution of wedge scattering to the radar cross section of the ocean surface," *IEEE Trans.* vol. GE-21, pp. 502–505, 1983.
93. L. B. Wetzel, "A minimalist approach to sea backscatter—the wedge model," in *URSI Open Symp. Wave Propagat.: Remote Sensing and Communication*, University of New Hampshire, Durham, preprint volume, July 28–August 1, 1986, pp. 3.1.1–3.1.4.
94. S. O. Rice, "Reflection of electromagnetic waves from slightly rough surfaces," *Commun. Pure Appl. Math.*, vol. 4, pp. 361–378, 1951.
95. W. H. Peake, "Theory of radar return from terrain," in *IRE Nat. Conv. Rec.*, vol. 7, 1959, pp. 27–41.
96. G. R. Valenzuela, "Depolarization of EM waves by slightly rough surfaces," *IEEE Trans.*, vol. AP-15, pp. 552–559, 1967.
97. F. G. Bass and I. M. Fuks, *Wave Scattering from Statistically Rough Surfaces*, New York: Pergamon Press, 1979.
98. C. Eckart, "The scattering of sound from the sea surface," *J. Acoust. Soc. Am.*, vol. 25, pp. 566–570, 1953.
99. P. Beckmann and A. Spizzichino, *The Scattering of Electromagnetic Waves from Rough Surfaces*, New York: Macmillan Company, 1963.
100. L. B. Wetzel, "HF sea scatter and ocean wave spectra," presented at URSI Spring Meet., National Academy of Sciences, Washington, April 1966.
101. A. K. Fung and G. W. Pan, "A scattering model for perfectly conducting random surfaces: I. model development," *Int. J. Remote Sensing*, vol. 8, no. 11, pp. 1579–1593, 1987.
102. G. R. Valenzuela, "Theories for the interaction of electromagnetic and oceanic waves—a review," *Boundary-Layer Meteorol.*, vol. 13, pp. 61–85, 1978.
103. B. F. Kuryanov, "The Scattering of sound at a rough surface with two types of irregularity," *Sov. Phys. Acoust.*, vol. 8, pp. 252–257, 1963.
104. W. J. Plant, "Bragg scattering of electromagnetic waves from the air/sea interface," in *Surface Waves and Fluxes: Current Theory and Remote Sensing*, chap. 12, G. L. Geernaert and W. J. Plant (eds.), Dordrecht, Netherlands: Reidel, 1988.
105. A. Schmidt, V. Wismann, R. Romeiser, and W. Alpers, "Simultaneous measurements of the ocean wave radar modulation transfer function at L, C and X bands from the research platform Nordsee," *J. Geophys. Res.*, vol. 100, pp. 8815–8827, 1995.
106. W. P. Plant, "A stochastic, multiscale model of microwave backscatter from the ocean," *J. Geophys. Res.*, vol. 107, no. C9, p. 3120, 2002.
107. V. Kudryavtsev, D. Hauser, G. Caudal, and B. Chapron, "A semiempirical model of the normalized radar cross-section of the sea surface 1. Background model," *J. Geophys. Res.*, vol. 108, no. C3, 8054, 2003.
108. V. Kudryavtsev, D. Hauser, G. Caudal, and B. Chapron, "A semiempirical model of the normalized radar cross-section of the sea surface 2. Radar modulation transfer function," *J. Geophys. Res.*, vol. 108, no. C3, 8055, 2003.
109. E. F. Knott, J. F. Shaeffer, and M. T. Tuley, *Radar Cross Section*, 2nd Ed., Boston: Artech House, 1993.
110. M. S. Longuet-Higgins and J. S. Turner "An 'entraining plume' model of a spilling breaker," *J. Fluid Mech.*, vol. 63, pp. 1–20, 1974.

111. K. J. Sangston, "Toward a theory of ultrawideband sea scatter," in *IEEE National Radar Conference 1997*, May 13–15, 1997, pp. 160–165.
112. D. Trizna (private communication), 1989.
113. J. C. West and M. A. Sletten, "Multipath EM scattering from breaking waves at grazing incidence," *Radio Sci.*, vol. 32, no. 3, pp. 1455–1467, 1997.
114. M. A. Sletten and J. C. West, "Radar investigations of breaking water waves at low grazing angles with simultaneous high-speed optical imagery," *Radio Sci.*, vol. 38, no. 6, p. 1110, 2003.
115. J. Chen, T. Lo, J. Litva, and H. Leung, "Scattering of electromagnetic waves from a time-varying fractal surface," *Microwave and Optical Tech. Lett.*, vol. 6, no. 1, p. 87, 2003.
116. S. Haykin, "Radar clutter attractor: implications for physics, signal processing and control," *IEE Proc. Radar: Sonar Navig.*, vol. 146, no. 4, p. 177, August 1999.
117. R. Harrington, *Time-Harmonic Electromagnetic Fields*, New York: McGraw-Hill, 1961.
118. D. J. Donohue, H-C Ku, D. R. Thompson, and J. Sadowski, "Direct numerical simulation of electromagnetic rough surface and sea scattering by an improved banded matrix iterative method," *Johns Hopkins APL Tech. Digest*, vol. 18, no. 2, pp. 204–215, 1997.
119. C. L. Rino and H. D. Ngo, "Numerical simulation of low-grazing-angle ocean microwave backscatter and its relation to sea spikes," *IEEE PGAP*, vol. 46, no. 1, 133–141, 1998.
120. J. C. West, J. M. Sturm, and A-J Ja: Low-Grazing Scattering from Breaking Water Waves Using an Impedance Boundary MM/GTD Approach, *IEEE Trans. Antennas Propagat.*, vol. 46, no. 1, pp. 93–100, January 1998.
121. D. B. Coakley, P. M. Haldeman, D. G. Morgan, K. R. Nicolas, D. R. Penndorf, L. B. Wetzel, and C. S. Weller, "Electromagnetic scattering from large steady breaking waves," *Experiments in Fluids*, vol. 30, no. 5, pp. 479–487, May 2001.
122. M. R. Keller, B. L. Gotwols, W. J. Plant, and W. C. Keller, "Comparison of optically-derived spectral densities and microwave cross-sections in a wind-wave tank," *J. Geophys., Res.*, vol. 100, no. C8, pp. 16163–16178, 1995.
123. E. A. Ericson, D. R. Lyzenga, and D. T. Walker, "Radar backscatter from stationary breaking waves," *J. Geophys. Res.*, vol. 104, Issue C12, p. 29679, 1999.
124. Y. G. Trokhimovski, "Gravity-capillary wave curvature spectrum and mean-square slope retrieved from microwave radiometric measurements (coastal ocean probing experiment)," *J. f Atmosph. Oceanic Tech.*, vol. 17, no. 9, pp. 1259–1270, 2000.

